



## JETS, DISKS AND THE DAWN OF PLANETS

Proceedings of the 2<sup>nd</sup> JEDI meeting  
(JEtS and DiSKs at INAF)

Capodimonte (Napoli), April 9-10, 2015



S. Antonucci, J. Alcalá, C. Codella, B. Nisini  
*Editors*

## Preface

This booklet contains a collection of contributions to the meeting of the JETs and Disks at INAF (JEDI) group, which took place at the Capodimonte Observatory during 9-10 April 2015. Scope of the meeting was to bring together the JEDI researchers of the Italian Istituto Nazionale di Astrofisica (INAF) working in the field of circumstellar disks and jets in young stars, to discuss together the different agents affecting the structure and the evolution of disks, namely accretion, jets and winds. More information on the JEDI group and its activities can be found at <http://www.oa-roma.inaf.it/irgroup/JEDI>. The JEDI group is supported through funds from the PRIN-2012 “*Disks, jets and the dawn of planets*”.

## List of participants:

Alcalá Juan M., *INAF – Osservatorio Astronomico di Capodimonte, Napoli, Italy*  
Antoniucci Simone, *INAF – Osservatorio Astronomico di Roma, Monte Porzio Catone, Italy*  
Biazzo Katia, *INAF – Osservatorio Astrofisico di Catania, Italy*  
Bacciotti Francesca, *INAF – Osservatorio Astrofisico di Arcetri, Firenze, Italy*  
Bianchi Eleonora, *INAF – Osservatorio Astrofisico di Arcetri, Firenze, Italy*  
Bonito Rosaria, *Università di Palermo, Italy*  
Codella Claudio, *INAF – Osservatorio Astrofisico di Arcetri, Firenze, Italy*  
Covino Elvira, *INAF – Osservatorio Astronomico di Capodimonte, Napoli, Italy*  
Fedele Davide, *Max-Planck-Institut für extraterrestrische Physik, Garching bei München, Germany*  
Fontani Francesco, *INAF – Osservatorio di Arcetri, Firenze, Italy*  
Frasca Antonio, *INAF – Osservatorio Astrofisico di Catania, Italy*  
Giannini Teresa, *INAF – Osservatorio Astronomico di Roma, Monte Porzio Catone, Italy*  
Guidi Greta, *INAF – Osservatorio Astrofisico di Arcetri, Firenze, Italy*  
Manara Carlo F., *ESA – ESTEC, Noordwijk, The Netherlands*  
Nisini Brunella, *INAF – Osservatorio Astronomico di Roma, Monte Porzio Catone, Italy*  
Podio Linda, *INAF – Osservatorio Astrofisico di Arcetri, Firenze, Italy*  
Rigliaco Elisabetta, *ETH – Institute for Astronomy, Zurich, Switzerland*  
Stelzer Beate, *INAF – Osservatorio Astronomico di Palermo, Italy*  
Tazzari Marco, *European Southern Observatory, Garching bei München, Germany*

# Contents

<b>Part 1: Early Protostellar Phases</b>	<b>4</b>
<i>E. Bianchi</i> – The $\text{CH}_3\text{CHO}/\text{HDCO}$ ratio as a tool to study the COMs formation . . . . .	5
<i>C. Codella</i> – HH212’s Anatomy: story of a protostellar series . . . . .	7
<i>F. Fontani</i> – Deuterated molecules: a chemical filter for shocks . . . . .	9
<b>Part 2: Disk Accretion and YSOs</b>	<b>11</b>
<i>J. M. Alcalá</i> – Search for accreting planets in transitional discs . . . . .	12
<i>S. Antoniucci</i> – HI decrements and line profiles in young stellar objects . . . . .	14
<i>K. Biazzo</i> – A study of accretion in the L1615/L1616 cometary cloud . . . . .	16
<i>D. Fedele</i> – Mass accretion in pre-main-sequence stars: the core strikes back . . . . .	18
<i>A. Frasca</i> – A study of young stellar objects in the $\gamma$ Velorum and Cha I clusters . . . . .	19
<i>T. Giannini</i> – EXORCISM: EXOR optiCal-Infrared Systematic Monitoring . . . . .	21
<i>C. F. Manara</i> – Accretion and wind proxies throughout disk evolution . . . . .	23
<i>E. Rigliaco</i> – Investigating Mid-Infrared Hydrogen lines as accretion indicators . . . . .	25
<b>Part 3: Jets and Winds</b>	<b>26</b>
<i>F. Bacciotti</i> – Effects of asymmetric jets on the dynamics of protoplanetary disks: study of a simple model . . . . .	27
<i>R. Bonito</i> – Shocks in accretion/ejection processes: observations, models, and laboratory experiments . . . . .	29
<i>T. Giannini</i> – The chemical inventory of HH1 . . . . .	31
<i>B. Nisini</i> – Connection between jets, winds, and accretion in T Tauri stars . . . . .	33
<b>Part 4: Physical and Chemical Properties of Disks</b>	<b>35</b>
<i>L. Podio</i> – Disks and jets with ALMA: sculpting the birthplace of exoplanets . . . . .	36
<i>M. Tazzari</i> – A new fitting tool to constrain dust grain size distribution and disk properties with ALMA and JVLA observations . . . . .	38

## **Part 1:**

### ***Early Protostellar Phases***

## THE CH<sub>3</sub>CHO/HDCO RATIO AS A TOOL TO STUDY THE COMS FORMATION

E. Bianchi<sup>1</sup>, C. Codella<sup>1</sup>, F. Fontani<sup>1</sup>, L. Testi<sup>1,2</sup>, R. Bachiller<sup>3</sup>, C. Ceccarelli<sup>4,5</sup>, B. Lefloch<sup>4,5</sup>, <sup>1</sup>*INAF - Osservatorio Astrofisico di Arcetri, Firenze, Italy*, <sup>2</sup>*European Southern Observatory, Garching, Germany*, <sup>3</sup>*IGN Observatorio Astronómico Nacional (IGN), Madrid, Spain*, <sup>4</sup>*Univ. Grenoble Alpes, IPAG, Grenoble, France*, <sup>5</sup>*CNRS, IPAG, Grenoble, France*.

Understanding the emergence of molecular complexity, from simple atoms and molecules to the large number of chemical species observed in the Solar System, is a crucial astrophysical topic. Complex Organic Molecules (COMs, > 6 atoms) have been detected in all the components of the star formation process, demonstrating the existence of efficient pathways to chemical complexity. During the low-mass star forming process, the primordial cloud evolves into a protostellar envelope, protoplanetary disk and planetary system. At the same time the interstellar medium evolves toward denser condensations and molecules can therefore be formed, destroyed or incorporated at the various stages so that the chemical composition of the gas becomes increasingly more complex.

One of the simplest COMs is acetaldehyde (CH<sub>3</sub>CHO). It has been recently detected in the chemically rich outflow driven by the L1157 mm protostar (Class 0), and associated with molecular clumpy cavities created by episodic events in a precessing jet. In particular, acetaldehyde has been revealed toward its brightest bow-shock called B1. Interestingly CH<sub>3</sub>CHO shows the same spatial distribution of deuterated formaldehyde (HDCO), both following the young outflow cavity produced by the impact of the jet with the ambient medium [4,3]. These observations indicated that the two molecules are closely associated with the region enriched by species evaporated from icy grain mantles and released into the gas phase.

In order to verify this result, we aim to extend the sample analyzing other three young stellar objects: SVS13 A & B, Cep E and HH212. We present here the preliminary results of the deuterated formaldehyde (HDCO) observations toward SVS13.

This object is located in the NGC1333 star forming region at a distance of 235 pc [5]. It is associated with several young stellar objects and in particular with two main bright mm-sources called A and B. SVS13A is thought to be a Class I object while SVS13B should be younger (Class 0) as suggested by the occurrence of a collimated jet [1].

Spectra of SVS 13A were observed with the IRAM 30-m antenna, in the framework of the ASAI large program (PI: B. Lefloch & R. Bachiller), an unbiased spectral survey aimed to observe several targets sampling different stages of solar-type star formation. As a first step we searched for the HDCO rotational transitions in the spectra at 1mm, 2mm, 3mm, using the GILDAS package<sup>1</sup> and the JPL<sup>2</sup> database to identify

the lines. We clearly detected four lines in the 1mm spectra one at 2mm, while the 3mm band did not present any HDCO transition. This could be due to a beam filling factor effect (HPBW  $\sim 10''$ ,  $20''$ ,  $30''$  at 1, 2, 3 mm, respectively). If the emitting size is significantly smaller than the beam size then the emission could be diluted. Note that the HPBW at 1mm is smaller than the angular separation ( $\sim 14.5$  arcsec) between the two main sources and samples only SVS13A. The preliminary analysis of the 1mm spectra shows four spectral lines (up to  $E_U \sim 40$  K) with a peak velocity of  $\sim 8$  km/s and typical FWHM of 2–4 km/s. Moreover some lines present an indication of a weak broader component that could be associated to an outflow. In Fig 1 we show the lines profile and the gaussian fit. In order to determine the excitation conditions i.e. excitation temperature and column densities, we build rotational diagrams of the different line components. This approach assumes that the lines are optically thin, and Local Thermodynamic Equilibrium (LTE). In Fig 2 we show the rotational diagrams. The green points indicate the bulk of the central line narrow emission around the peak velocity while the blue and the red points correspond respectively to the blue and the red broader wings. We found rotational temperatures of  $\sim 20$  K and column densities of  $N \sim 4 \times 10^{12} \text{ cm}^{-2}$  for the central emission,  $N \sim 3 \times 10^{11} \text{ cm}^{-2}$  for the blue wings and  $N \sim 5 \times 10^{10} \text{ cm}^{-2}$  for the red one. Further analysis will be carried out for the detection of the acetaldehyde (CH<sub>3</sub>CHO) in the same source and subsequently of both HDCO and CH<sub>3</sub>CHO in the other objects.

## References.

- [1] Bachiller, R., Guilloteau, S., Gueth, F., et al. 1998, A&A, 339, L49
- [2] Caselli P. & Ceccarelli C. 2012, A&A Rev, 20, 56
- [3] Codella C., Fontani F., Ceccarelli C., et al., 2015, MNRAS 449, L11
- [4] Fontani F., Codella C., Ceccarelli C., et al. 2014, ApJ 788, L43
- [5] Hirota, T., Bushimata, T., Choi, Y. K. et al. 2008, PASJ, 60, 37
- [6] Pickett, H. M., Poynter, R. L., Cohen, E. A., et al. 1998, JQSRT, 60, 883

<sup>1</sup><http://www.iram.fr/IRAMFR/GILDAS>

<sup>2</sup>Jet Propulsion Laboratory molecular database [6]

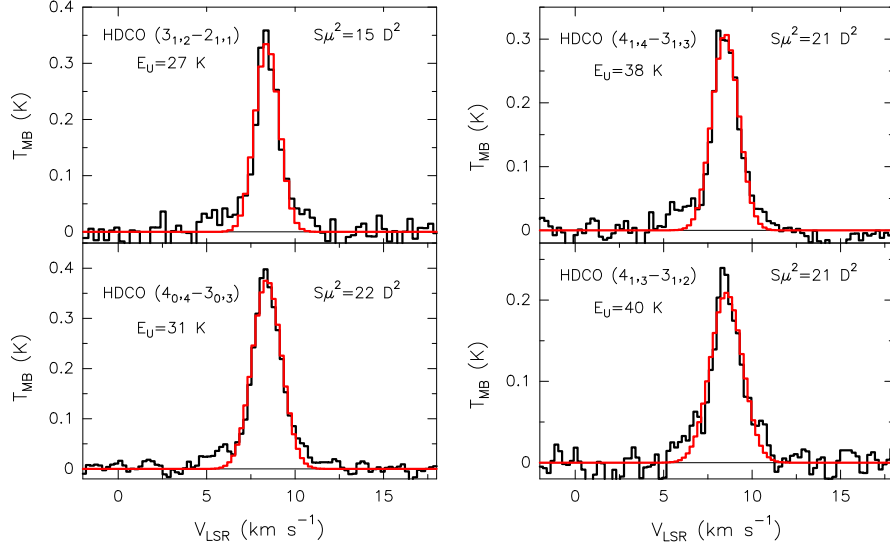


Figure 1: Deuterated formaldehyde (HDCO) detected spectral lines toward SVS13A. The lines were observed at 1 mm with the IRAM 30-m antenna, in the ASAI framework (PI: B. Lefloch & R. Bachiller). The spectra are reported in the main beam temperature scale. The peak velocity is  $\sim 8$  km/s, while the typical FWHM are 2–4 km/s. In red we show the gaussian fit of the spectral lines.

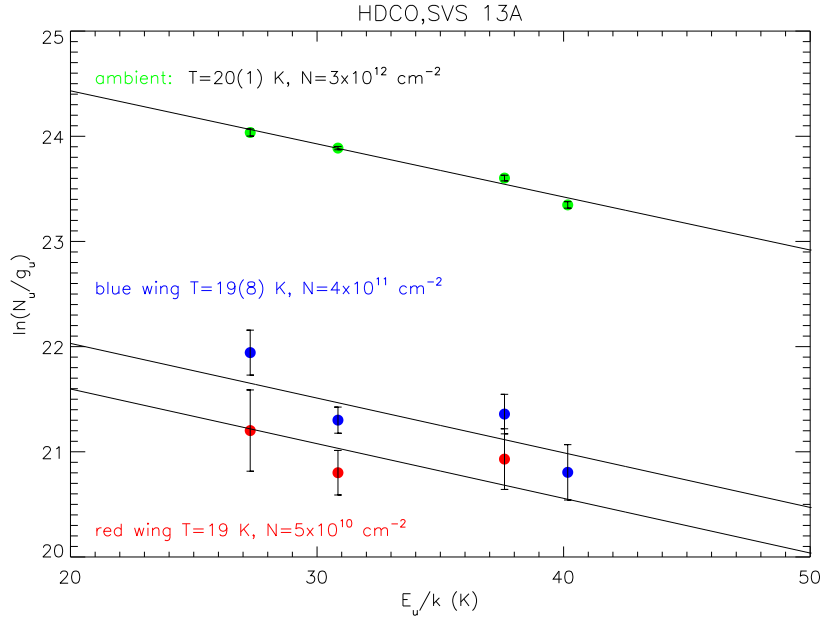


Figure 2: Rotational diagram for HDCO as observed toward SVS13A. The green points indicate the velocity range of  $\sim 5$  km/s around the peak velocity. The blue (red) points correspond to the blue (red) wings. The black lines are for the best fits. The values of both rotational temperatures and column densities are derived under the assumption of optically thin emission and LTE. For the red wings we assume the same rotational temperatures of the blue one.

## HH212'S ANATOMY: STORY OF A PROTOSTELLAR SERIES

C. Codella; *INAF - Osservatorio Astrofisico di Arcetri, Firenze, Italy.*

Magneto-hydrodynamical (MHD) driven jets play a crucial role during the earliest Class 0 phase, that is in the star and disk formation process itself. High-resolution MHD simulations of protostellar collapse show that MHD outflows are an unavoidable outcome, and are able to eject 20%–50% of the infalling core gas before it reaches the central source [2]. The magnetic braking by the outflows and twisted B-fields is so efficient when the field and the spin axis are aligned that keplerian disks may be initially suppressed beyond 10 AU (e.g. [9]). On the other hand, large keplerian disks of 100–150 AU have recently been reported in three Class 0 sources [11,10,8]. Such large Keplerian disks might result from misaligned  $B - \Omega$  configurations or a strong turbulence [5], but observational evidence is still lacking. A detailed observation and characterisation of a larger sample of Class 0 systems is thus essential to elucidate the disk formation process.

HH212 is a bright symmetric bipolar jet from a Class 0 source in Orion (e.g. [13]). Previous Sub-Millimeter Array (SMA) and Plateau de Bure Interferometer (PdBI) maps of the inner ( $\leq 900$  AU) region revealed a bipolar SiO/CO microjet invisible in  $H_2$  due to high extinction (e.g. [3,6,1]). The dust continuum recently imaged by ALMA suggests a disk of (maximum) radius  $\simeq 0.3$  AU [7]. All these findings make HH212 an ideal laboratory for investigating the interplay of infall, outflow and rotation in the protostellar stages.

We summarise here the first results obtained using HH212 observations performed during the ALMA Cycle 0 phase. The CO(3–2),  $C^{17}O(3-2)$ , SiO(8–7),  $C^{34}S(7-6)$ , and  $CH_3OH(7_{1,7}-6_{1,6})$  lines at 345795.99 MHz, 337061.13 MHz, 347330.63 MHz, 337396.69 MHz, and 335582.00 MHz respectively, were observed using spectral units of  $0.43 \text{ km s}^{-1}$  resolution. Further details can be found in [4].

Figure 1 compares the emission maps in the  $850 \mu\text{m}$  continuum, SiO(8–7), CO(3–2),  $C^{17}O(3-2)$ ,  $C^{34}S(7-6)$ , and  $CH_3OH(7_{1,7}-6_{1,6})$ . The combination of these tracers allows us to simultaneously image in a single ALMA–Band 7 spectral set-up different ingredients of the star formation process: (i) a pair of narrow SiO jets launched from the protostar (dust and  $CH_3OH$  peaks), (ii) an extended flattened  $C^{17}O$  envelope around the outflow waist, and (iii) biconical CO and  $C^{34}S$  emission lobes surrounding the jet.

Figure 2 shows that, in addition to infall motions (traced by the extended diamond shape of the position-velocity plot), a rotation signature is clearly seen in the form of two emission peaks at low velocities (LV;  $\leq 1.5 \text{ km s}^{-1}$ ): one blueshifted to the west, and one redshifted to the east. This rotating LV  $C^{17}O$  emission is tracing the sides of the southern cavity carved by the outflow into the envelope, which rotates in the same sense [12]. At high velocities (HV;  $\simeq 1.9\text{--}3.5 \text{ km s}^{-1}$  from systemic): (i) the E-W velocity gradient is still present, and (ii) the emission is definitely more compact ( $\leq 0.5$  arcsec). We obtained the emission centroid positions in each channel from fits in the  $uv$  domain. While the centroids in the LV range fall on the southern cavity, the centroids in the HV range move to the equatorial plane, which indicates an inner rotating equatorial disk of radius  $\simeq 0.2$  arcsec (90 AU) around a  $0.3 \pm 0.1 M_{\odot}$  protostar.

### References.

- [1] Cabrit S., Codella C., Gueth F., & A. Gusdorf 2012, A&A 548, L2
- [2] Ciardi A., & Hennebelle P. 2010, A&A 409, L39
- [3] Codella C., Cabrit S., Gueth F., et al. 2007, A&A 462, L53
- [4] Codella C., Cabrit S., Gueth F., et al. 2014, A&A 568, L5
- [5] Joos M., Hennebelle P., & Ciardi A. 2012, A&A 543, 128
- [6] Lee C.-F., Ho P.T.P., Bourke T.L., et al. 2008, ApJ 685, 1026
- [7] Lee C.-F., Hirano N., Zhang Q., Shang H., Ho P.T.P., & Krasnopolsky R. 2014, ApJ 786, 114
- [8] Lindberg J.E., Jørgensen J.K., Brinch C., et al. 2013, A&A 566, A74
- [9] Machida M.N., Inutsuka S.-I., & Matsumoto T. 2011, PASJ 63, 555
- [10] Murillo N.M., Lai S.-P., Bruderer S., Harsolo D., & van Dishoeck E.F. 2013, A&A 560, A103
- [11] Tobin J., Hartmann L., Looney L.W., & Chiang H.-F. 2010, ApJ 712, 1010
- [12] Wiseman J., Wootten A., Zinnecker H., & McCaughrean M. 2001, ApJ 550, L87
- [13] Zinnecker H., McCaughrean M.J., & Rayner J.T. 1998, Nature 394, 862

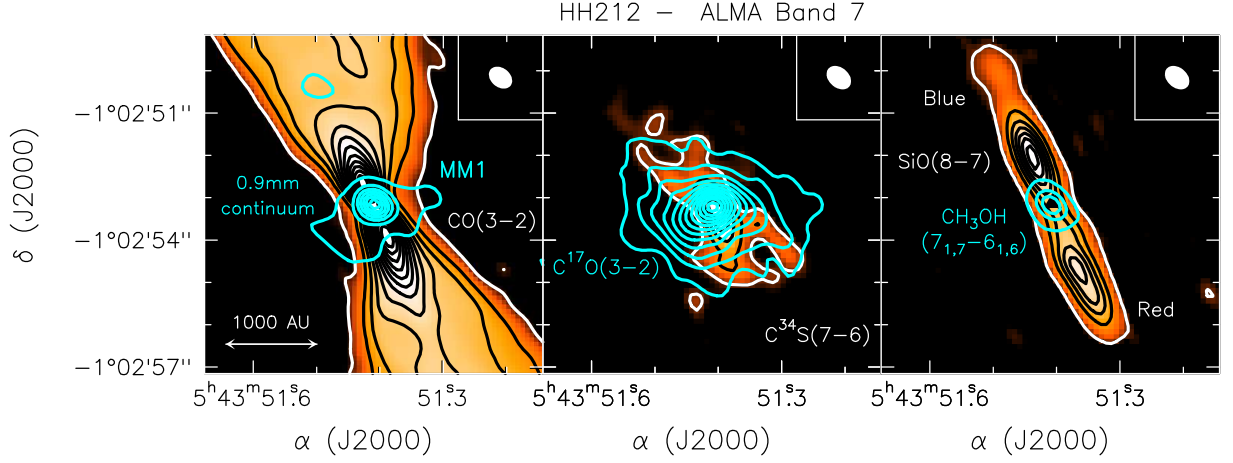


Figure 1: The HH212 protostellar system as observed with ALMA–Band 7 [4]. *Left panel:* Contour plot of the continuum emission (turquoise contours) at 0.9 mm overlaid on top of the CO(3–2) emission (colour scale and black contours), integrated in the  $V_{sys} \pm 17 \text{ km s}^{-1}$  range. The ellipse shows the ALMA synthesised beam (HPBW). Labels indicate the MM1 protostar. *Middle panel:* Contour plot of the  $C^{17}O(3-2)$  emission (turquoise) on top of the  $C^{34}S(7-6)$  emission (colour and black), both integrated in the  $V_{sys} \pm 6 \text{ km s}^{-1}$  range. *Right panel:* Contour plot of the  $CH_3OH(7_{1,7}-6_{1,6})$  emission (turquoise, integrated in the  $V_{sys} \pm 6 \text{ km s}^{-1}$  range) on top of the SiO(8–7) emission (colour and black, integrated between  $-23$  and  $+15 \text{ km s}^{-1}$  with respect to  $V_{sys}$ ).

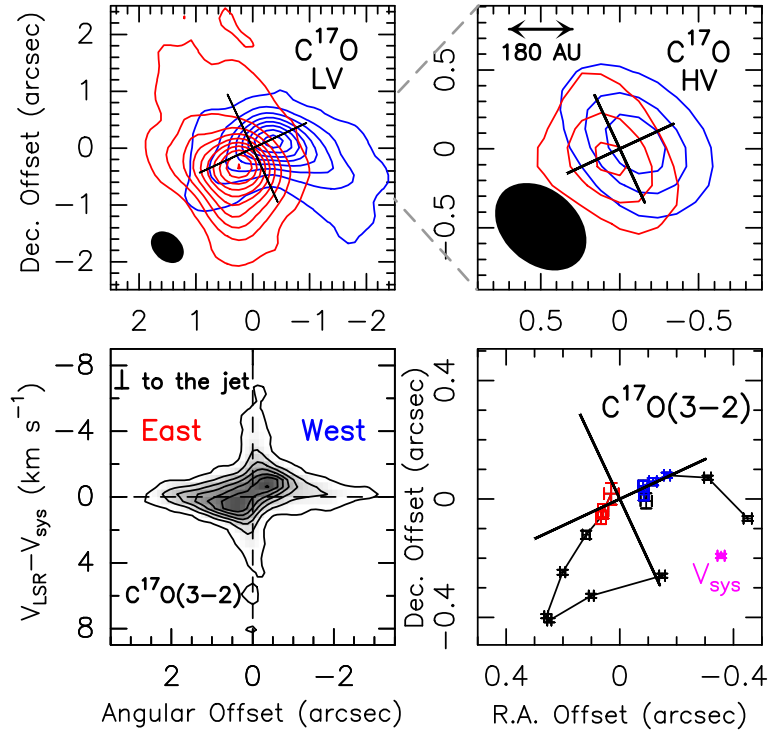


Figure 2: *Upper-left:* Blue- and redshifted  $C^{17}O(3-2)$  emission in the low-velocity (LV) range ( $\pm 0.6$ – $1.5 \text{ km s}^{-1}$  from  $V_{sys}$ ), tracing the rotating outflow cavity. The tilted black cross indicates the SiO jet direction ( $PA = 22^\circ$ ) and the equatorial plane. *Upper-right:* same as the Upper-left panel for the high-velocity (HV) velocity range ( $\pm 1.9$ – $3.5 \text{ km s}^{-1}$  from systemic), tracing the rotating inner disk. *Bottom-left:* position-velocity cut of  $C^{17}O(3-2)$  perpendicular to the jet. Dashed lines mark  $V_{sys}$  and the continuum peak MM1. *Bottom-right:* distribution of the  $C^{17}O(3-2)$  centroid positions (from fits in the  $uv$  domain with  $1\sigma$  error bars) in the various velocity channels. Magenta is used for the systemic velocity. Red and blue datapoints denote the channels whose fitted centroids lie, within the error bars, on the equator.

## DEUTERATED MOLECULES: A CHEMICAL FILTER FOR SHOCKS

F. Fontani; *INAF - Osservatorio Astrofisico di Arcetri, Firenze, Italy.*

The process of deuterium enrichment in molecules from the main reservoir HD is initiated in molecular clouds by exothermic gas-phase reactions, and it is thus boosted in cold and dense gas (e.g. [1]). For this reason, deuterated molecules have long been used as tracers of the coldest and densest portions of interstellar clouds. Although this general framework remains true, increasing observational evidence is showing that the story is not so simple: deuterium fractionation is boosted in cold and dense gas, but it does not uniquely trace cold and dense gas. In fact, a second very efficient way to form molecules rich in hydrogen and deuterium is on the surfaces of dust grains during the early cold pre-stellar phase, which are then released into the gas by thermal or non-thermal desorption mechanisms. Therefore, their abundance can reach high values even in hot gas (see [2] for a review). High deuterated fractions (i.e. the abundance ratio of the isotopologue containing D and its counterpart containing H) of species that are efficiently formed on dust grains, like formaldehyde, ammonia, and methanol, are indeed measured in hot-cores and hot-corinos (e.g. [2]), where evaporation of grain mantles due to heating of a protostellar object is maximum. However, up to now, the deuterated fraction in shocks was not investigated.

The first source in which this investigation has been performed is L1157-B1, the brightest bow-shock associated with the protostellar outflow L1157 (the prototype of chemically active outflows) driven by a low-mass class-0 protostar [3]. Towards L1157-B1, several emission lines of deuterated molecules have been detected by our team for the first time (including HDCO and CH<sub>2</sub>DOH) with the IRAM-30m Telescope [4]. Based on chemical models [5], we suggested that these species were formed on grain mantles, and then released into the gas phase by the passage of the shock. The young age of the shock ( $\sim 2000$  yrs, [6]) is consistent with this picture, because in such a short lifetime the chemical reactions in the hot gas unlikely can modify significantly the chemical composition of the evaporated material (e.g. [7]). However, the angular reso-

lution of the data published by [4] was not sufficient to firmly claim that the detected emission indeed arises from the shock impacting region. This scenario has been fully confirmed by observations obtained at high angular resolution with the Plateau de Bure Interferometer [8]: as expected the emission of HDCO perfectly delineates the region of interface between the fast jet and the slower ambient material (Fig. 1). CH<sub>2</sub>DOH emission is fainter and thus its emitting region is not as clearly delineated as for HDCO, but its integrated map is consistent with gas mainly ejected where the jet impinges the ambient material. The deuterated fraction HDCO/H<sub>2</sub>CO is  $\sim 0.1$  in the HDCO emitting region, an order of magnitude larger than the upper limit found in the surrounding material, probably dominated by warm-gas chemistry and less affected by grain evaporation. Our study represents the first clear evidence ever found of HDCO as shock tracer, proposing a new use of this molecule as "chemical filter" to trace recently evaporated material (more selective than its hydrogenated counterpart, as it can be seen from Fig. 1). Moreover, the study yields an indirect but "clean" measurement of the deuteration of the ices covering the dust grains during the cold pre-protostellar phase.

### References.

- [1] Millar et al. 1989, ApJ, 340, 906
- [2] Caselli & Ceccarelli 2012, A&ARv, 20, 56
- [3] Bachiller et al. 2001, A&A, 372, 899
- [4] Codella et al. 2012, ApJ, 757, L9
- [5] Taquet et al. 2012, ApJ, 784, L3
- [6] Gueth et al. 1996, A&A 307, 891
- [7] Osamura et al. 2004, A&A, 421, 1101
- [8] Fontani et al. 2014, ApJ, 788, L43
- [9] Benedettini et al. 2013, MNRAS, 436, 179
- [10] Codella et al. 2009, A&A, 507, L25

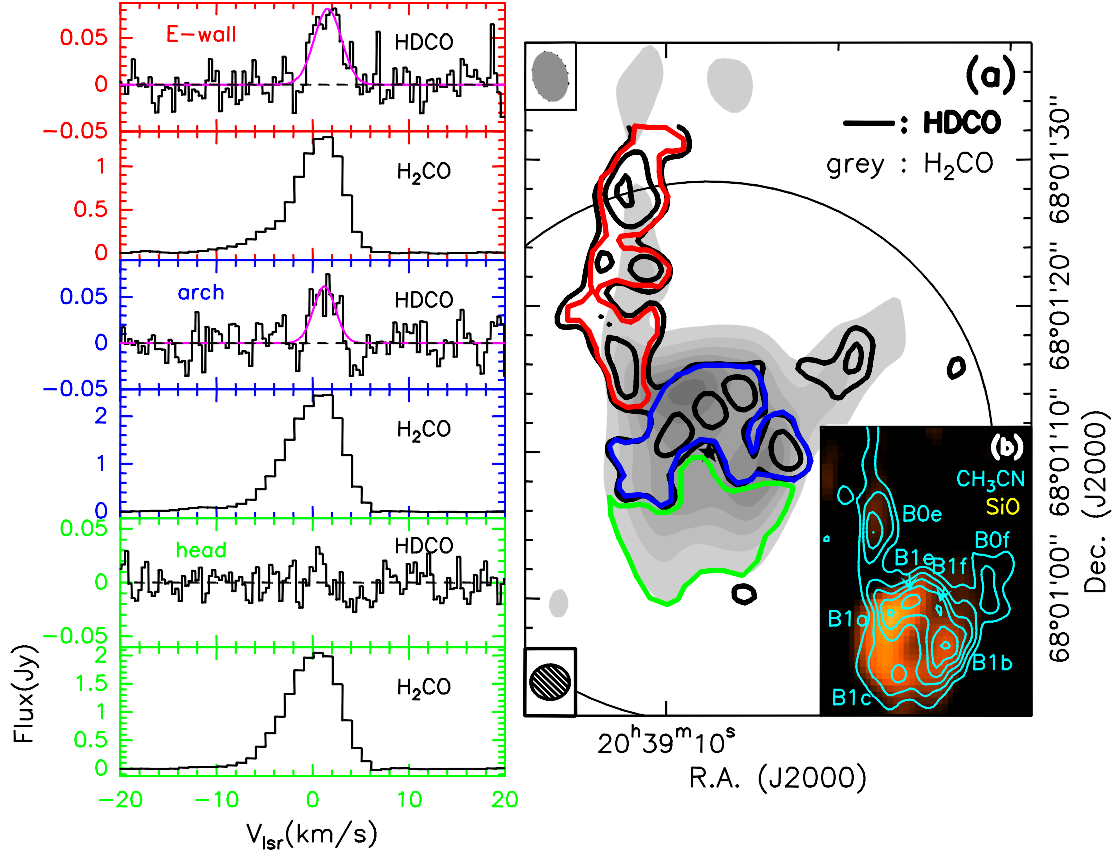


Figure 1: (a): map of the intensity of the HDCO(2<sub>1,1</sub> - 1<sub>0,1</sub>) line (thick black contours) averaged between -0.7 and 3.4 km s<sup>-1</sup>, observed with the PdBI. Contours are 3, 5 and 7 times the 1σ rms level in the map, i.e. ~ 3.8 mJy beam<sup>-1</sup>. The grey scale represents the averaged emission of H<sub>2</sub>CO(2<sub>0,2</sub> - 1<sub>0,1</sub>) observed with the PdBI by Benedettini et al. [9]: the levels range from 15 (3σ rms level) to 190 mJy beam<sup>-1</sup>, in steps of 30 mJy beam<sup>-1</sup>. The big circle represents the PdBI primary beam (~ 37'') at the frequency of the HDCO line, and the ellipses in the bottom- and top-left corners show the PdBI synthesised beam for the HDCO and H<sub>2</sub>CO images, respectively. (b): SiO(2-1) (heat colour scale) and CH<sub>3</sub>CN(8-7) (K=0-2, cyan contours) averaged emission, with the location of the CH<sub>3</sub>CN condensations identified by Codella et al. ([10], same contour levels as in their Fig. 1 are shown). To the left of the maps, we show the spectra of HDCO(2<sub>1,1</sub> - 1<sub>0,1</sub>) and H<sub>2</sub>CO(2<sub>0,2</sub> - 1<sub>0,1</sub>) integrated over the red, blue and green contours (from top to bottom) in panel (a). These delineate: the eastern wall ("E-wall") of the cavity detected in HDCO, the arch-like structure ("arch") detected in HDCO behind the head of the bow-shock, and the "head" of the bow-shock detected in H<sub>2</sub>CO but not in HDCO. The purple line in the HDCO spectra shown in the "E-wall" and "arch" panels represents the best Gaussian fit to the lines. From [8].

## **Part 2:**

### ***Disk Accretion and YSOs***

## SEARCH FOR ACCRETING PLANETS IN TRANSITIONAL DISCS

J.M. Alcalá<sup>1</sup>, E. Covino<sup>1</sup>, S. Antonucci<sup>2</sup>, B. Nisini<sup>2</sup>, T. Gianinni<sup>2</sup>, C. Manara<sup>3</sup>; <sup>1</sup>INAF - Osservatorio Astronomico di Capodimonte, Napoli, Italy, <sup>2</sup>INAF - Osservatorio Astronomico di Roma, Monte Porzio Catone, Italy, <sup>3</sup>ESA/ESTEC, Noordwijk, The Netherlands.

A key issue in the study of planet formation is to explain how optically thick accretion discs surrounding the youngest solar-mass stars, i.e. the classical T Tauri stars, evolve into optically thin debris discs around young main sequence stars, passing through the weak-T Tauri star phase [22]. Generally, these discs persist for several million years [11], during which part of the material is accreted onto the star, part is lost via outflows and photoevaporation, and part condenses into centimeter-sized and larger bodies or planetesimals. An intermediate stage of T Tauri disc evolution is observationally identified with the so-called "transitional discs" (TDs), which are characterised by inner holes in their dust distribution. The analysis of the spectral energy distribution (SED) and interferometric measurements at sub-millimeter wavelengths indicate inner cavity radii,  $R_{in}$ , spanning from a few AU to several tens of AU [9,2,16,10].

Important clues to the process of planet formation are expected from observation of TDs, as they represent the best candidate places where forming planets can be found, located inside the circumstellar disc cavity and close to the inner rim of the disc [7]. Therefore, the estimates of  $R_{in}$  provide upper limits for the expected orbital radius of the planet, although depending on the SED modelling approach used [12,20]. Therefore, direct detection of the inner rim of TDs is also crucial to constrain the models.

### 1. Accreting planets in TDs

Recent measurements of high mass-accretion rates ( $\dot{M}_{acc} \sim 10^{-9} - 10^{-8} M_{\odot} \text{yr}^{-1}$ ; [9,15,1]) in several TDs (see Fig. 1) suggest that there may still be an important amount of residual circumstellar gas in the inner cavity. Interestingly, no correlation is found between  $\dot{M}_{acc}$  and the size of the inner cavity (Fig. 1, bottom panel), as would be expected for magnetospheric accretion onto the star. This suggests that the density of the gas in the inner regions is independent of the mechanisms producing the cavity [15]. Therefore, the accretion activity has also been ascribed to mass accretion onto forming planets [14,18,24]. Indeed, since circumstellar discs have lifetimes of some million years, forming a  $1-10 M_{Jup}$  planet during this time lapse requires that a *circumplanetary disc* has an average accretion rate of  $\dot{M}_{acc} \geq 10^{-9} - 10^{-8} M_{\odot} \text{yr}^{-1}$ . However, except for the candidates around LkCa 15 [13], HD100546 [17] and HD169142 [19,5], objects showing evidences of on-going planet formation have not been clearly detected yet.

### 2. Detection of circumplanetary discs

Recent calculations [24,8] of the SEDs of circumplanetary accretion discs have shown that a circumplanetary disc with  $\dot{M}_{acc} \approx 10^{-8} M_{\odot} \text{yr}^{-1}$ , around a  $1 M_{Jup}$  planet has a maximum temperature of  $\sim 2000$  K, and in the near-infrared it

should be as bright as a late-type brown dwarf or as a  $\sim 10 M_{Jup}$  planet. Hence, such a disc could be detected by using the high-contrast, high angular resolution and high sensitivity instrument SPHERE@VLT. However, in order to identify unambiguously circumplanetary accretion and distinguish it from brown dwarf companions or hot high-mass planets, we need to reveal accretion signatures such as  $H\alpha$  emission, and/or find indication from mid-infrared photometry of a flatter SED, caused by a warm circumplanetary disc, as compared to the SED of brown dwarfs or non-accreting planets [24]. Recent studies have stressed on the use of  $H\alpha$  emission as a powerful diagnostic to find both accreting stellar companions [6] and proto-Jupiters [23].

### 3. The project

Detecting and characterising planetary-mass companions of young stellar objects (YSOs) with TDs and studying the dust distribution in the inner disc rims are primary observational steps for unveiling planet formation processes and for constraining the models of late disc evolution. Therefore, within the framework of JEDI we have started a project to investigate YSOs with TDs using SPHERE@VLT and LMIRCam@LBTI, in close collaboration with the INAF-Padova group in charge of high-contrast, high spatial resolution imaging techniques. The main goal of this project is to look for planetary-mass companions around YSOs with TDs. The YSOs span a narrow range of ages, between 1 Myr and 3 Myr, and show evidence of mass-accretion, which makes them the best candidates to host forming planets. Planetary companions are expected to be located inside the cavities of the TDs and close to the inner edge of the disc cavity [7].

### References.

- [1] Alcalá et al. 2014 A&A, 561, 2
- [2] Andrews et al. 2011 ApJ, 732, 42A
- [3] Bustamante et al. 2015arXiv150105204
- [4] Baraffe et al. A&A, 402, 701
- [5] Biller et al. ApJ, 792, 22
- [6] Close et al. 2014, ApJ, 781, 30
- [7] de Juan Ovelar et al. 2013, A&A, 560, 111
- [8] Eisner 2015, arXiv150205412
- [9] Espaillat et al. 2010, ApJ, 717, 441
- [10] Espaillat et al. 2014, prpl.conf.497
- [11] Fedele et al. 2010, A&A 510, 72
- [12] Kim et al. 2009 ApJ, 700, 1017
- [13] Kraus & Ireland 2012 ApJ, 745, 5
- [14] Lubow et al. 1999 ApJ, 526, 1001
- [15] Manara et al. 2014 A&A, 568, 18
- [16] Pinilla et al. 2012 A&A, 545, 81

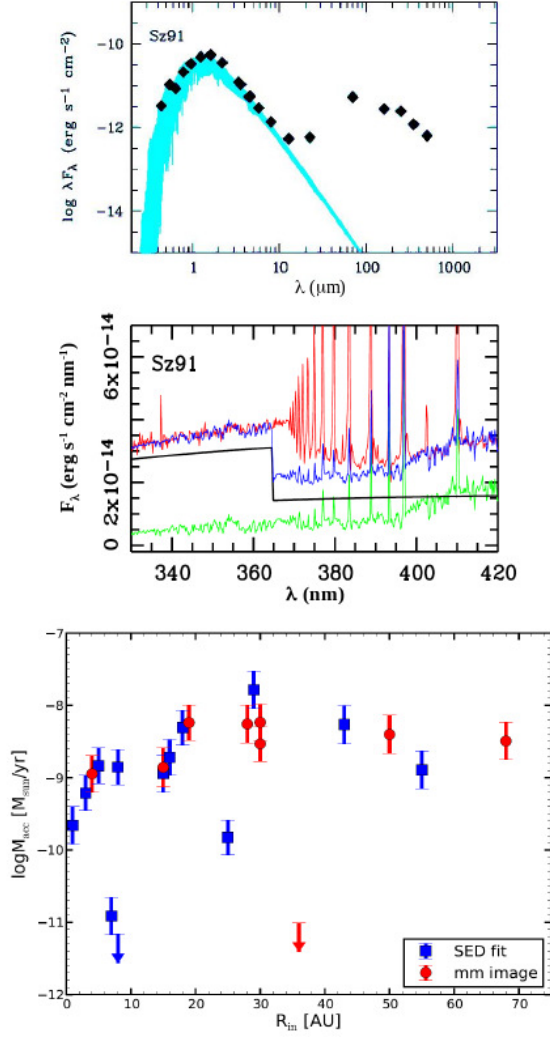


Figure 1: *Top*: typical SED of a TD for the YSO Sz91 in Lupus III (black symbols). A model atmosphere of the same effective temperature as the star is overplotted (blue line). The "valley" between 10 μm and 100 μm due to the lack of dust in the inner disc regions is clearly seen. The estimated size of the inner cavity is  $R_{in} = 65$  AU ([21]). *Middle*: UVB X-Shooter spectrum of Sz91 (red) showing the noticeable accretion signatures as UVB excess emission and Balmer jump with respect to a template discless star of the same spectral-type (green). A mass accretion rate  $\dot{M}_{acc} = 1.5 \times 10^{-9} M_\odot \text{yr}^{-1}$  was calculated by fitting (blue line) the template plus the emission of a slab of hydrogen (black) (adapted from [1]). *Bottom*:  $\dot{M}_{acc}$  versus radius of the inner cavity of a sample of TDs (adapted from [15]).

- [17] Quanz et al. 2013 ApJ, 766, 1
- [18] Owen 2014 ApJ, 789, 59
- [19] Reggiani et al. 2014 ApJ, 792, 23
- [20] Rodgers-Lee et al. 2014MNRAS,443,1587
- [21] Tsukagoshi et al. 2014,ApJ,783,90
- [22] Williams & Cieza 2011 ARA&A,49, 67
- [23] Zhou et al. 2014 ApJ, 783, 17
- [24] Zhu 2015 ApJ, 799, 16

# HI DECREMENTS AND LINE PROFILES IN YOUNG STELLAR OBJECTS

S. Antonucci; *INAF - Osservatorio Astronomico di Roma, Monte Porzio Catone, Italy.*

Hydrogen recombination lines (HI) are one of the most common features observed in optical and near-infrared spectra of young stellar objects (YSOs) and represent a powerful tracer for the high-density gas located in the innermost circumstellar region of young stars. These lines are commonly used as a tracer of the mass accretion process [1,2], but they can also be effectively employed to probe the physical properties of the gas in the circumstellar structures [6,10,11]. Instruments like VLT/X-Shooter, with its broad wavelength coverage and moderate spectral resolution, allow us now to *simultaneously* study HI lines from the Balmer, Paschen, and Brackett series, and to derive both the stellar and accretion properties of the young sources from the analysis of spectral features and accretion-related excess emission [1,9].

In our work [3] we have considered the X-Shooter spectra presented by [1], which refer to a sample of 36 low-mass Class II sources in the Lupus low-mass star-forming region [5] for which all the stellar and accretion properties are already available. Thanks to the good quality of the UVB and VIS spectra of this X-Shooter dataset, we have focused on the lines of the Balmer series, and in particular on the analysis of the series decrement. On the one hand, we have looked for correlations between the decrement shape, the observed line profiles, and the (stellar and accretion) properties of the objects; on the other hand we have compared the observed decrements to the predictions of standard emission models (case B [7], and the *local line excitation computations* by [8]). Our aim is to investigate what are the gas properties in the line emission region and whether these vary throughout the sample.

## 1. Decrement shapes

The extinction-corrected Balmer decrements of the targets relative to the  $H\beta$  ( $H4$ ) line and up to the  $H15$  line are shown in Fig. 1. Although the decrement shapes vary with continuity within the sample, we have identified four major decrement types, which are reported in the panels of Fig. 1, using a representative source for each type. Only three objects present a type 1 decrement, which presents a curved shape outlining the lower part of the decrement ensemble. Type 2 decrements are the most common (20/36) and look as roughly straight lines in the plot. Type 3 decrements (7/36) have a shape characterised by a fairly wide bump and unlike type 1s occupy the upper side of the decrement ensemble. Finally, in type 4 (6/36) the slope is steep for the first lines of the series and becomes flatter for  $N_{up} \geq 6$ .

## 2. Decrements and source properties

We note that the three sources displaying type 1 decrements have been previously identified as sub-luminous objects [1], most likely due to geometrical obscuration of the central region from an edge-on view of the disc. In such a geometry it is likely

to have a residual amount of (differential) extinction that is not properly accounted for, which would effectively result in a type 1 shape decrement.

We could not determine any clear correlation between the other decrement shapes and the source properties, except for a tentative connection with the mass accretion rate. Indeed, the strongest accretors in the sample seem to show similar decrement shapes: type 4 (mostly) and type 2.

## 3. Decrements and line profiles

Twelve targets present highly symmetric lines with a FWHM around 100 km/s (*narrow symmetric line objects*). Much larger profiles (FWHM up to 350-400 km/s) that are still symmetric are observed in eight sources, while the remaining sources show more complex (double- or triple-peaked) profiles, as a result of strong absorptions. The FWZI measured in the sample are in the range 400-1600 km s<sup>-1</sup>. The comparison between FWHM and FWZI indicate that most objects have lines that significantly differ from a Gaussian, having very extended wings, which may signal gas moving at very large velocities with respect to the star. The most evident connection between decrement shape and line profiles is that all sources with narrow symmetric lines display a type 2 decrement, although not all type 2 decrements are associated with narrow symmetric line objects. Targets with type 4 decrements have in general very wide profiles, which suggests emission from a fairly extended circumstellar region in which large amounts of gas move at different velocities, a picture that is consistent with the connection between type 4 decrements and higher mass accretion rates.

## 4. Decrements and models

Case B emission is able to reproduce well type 2 and type 3 decrements assuming large densities ( $> 10^{10}$  cm<sup>-3</sup>) and low temperatures (1000-2000 K) [4], but in order to satisfy the assumptions of case B (optically thin lines) under these conditions a very strong source of ionising photons is required, which is hardly found in circumstellar regions of typical T Tauri stars.

Models by [7] can manage optically thick lines, although in a *local* environment, i.e. assuming a gas with a single temperature and density, a velocity gradient, and an ionisation rate. These models reproduce well sources with type 4 decrements, indicating (total) densities around  $10^{10}$ - $10^{11}$  cm<sup>-3</sup> and temperatures around 10000 K. This suggests that in this sources the bulk of the emitting gas is well described in terms of a single temperature and density. The most common type 2 decrements are reproduced less well at somewhat lower gas densities ( $10^9$ - $10^{10}$  cm<sup>-3</sup>), while the temperature remains difficult to constrain. Type 3 decrements remain the most difficult to reproduce in the framework of these models.

A more complex modelling of the emitting region (including a temperature and density profile) is probably required to

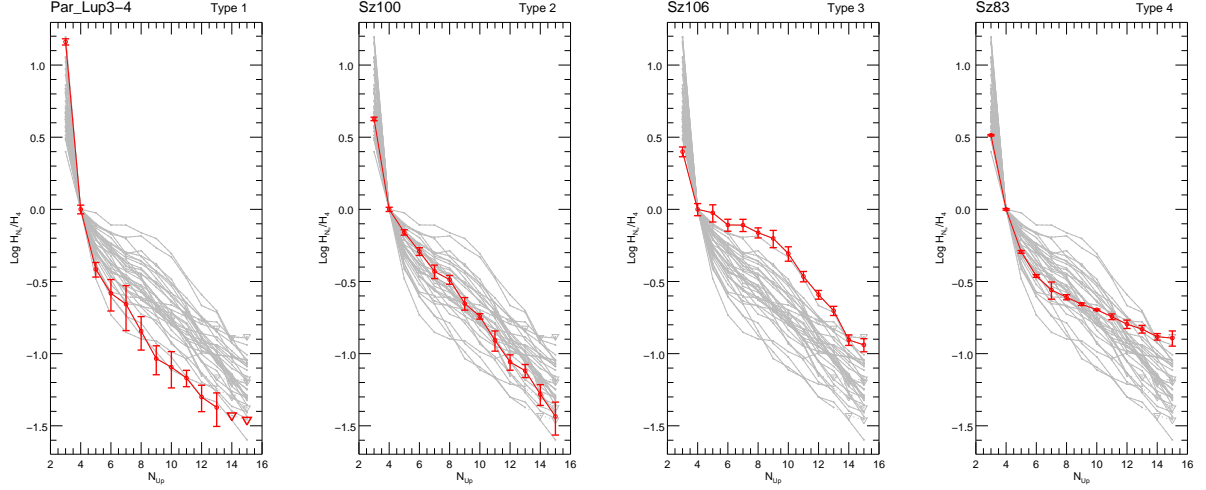


Figure 1: Balmer decrements of four sources of the Lupus sample. Each target represents one of the four main decrement shapes we have identified, which are plotted in red against the ensemble of all decrements of the sample (grey curves). Adapted from [2].

fully reproduce the observed decrements and derive the properties of the emitting gas.

#### References.

- [1] Alcalá, J. M., Natta, A., Manara, C. F., et al. 2014, *A&A*, 561, A2
- [2] Antonucci, S., Rigliaco, E., et al. 2015, in preparation
- [3] Antonucci, S., García López, R., Nisini, B., et al. 2014, *A&A*, 572, A62
- [4] Bary, J. S., Matt, S. P., Skrutskie, M. F., et al. 2008, *ApJ*, 687, 376
- [5] Comeron, F. 2008, in *Handbook of Star Forming Regions, Vol. II: The Southern Sky* ASP Monograph Publications (Bo Reipurth), 295
- [6] Edwards, S., Kwan, J., Fischer, W., et al. 2013, *ApJ*, 778, 148
- [7] Hummer, D. G., & Storey, P. J. 1987, *MNRAS*, 224, 801
- [8] Kwan, J., & Fischer, W. 2011, *MNRAS*, 411, 2383
- [9] Manara, C. F., Beccari, G., Da Rio, N., et al. 2013, *A&A*, 558, A114
- [10] Nisini, B., Antonucci, S., & Giannini, T. 2004, *A&A*, 421, 187
- [11] Whelan, E. T., Bonito, R., Antonucci, S., et al. 2014, *A&A*, 565, A80

## A STUDY OF ACCRETION IN THE L1615/L1616 COMETARY CLOUD

K. Biazzo<sup>1</sup>, J. M. Alcalá<sup>2</sup>, A. Frasca<sup>1</sup>, M. Zusi<sup>3</sup>, F. Getman<sup>1</sup>, E. Covino<sup>1</sup>, D. Gandolfi<sup>4</sup>; <sup>1</sup>INAF - Osservatorio Astrofisico di Catania, Italy, <sup>2</sup>INAF - Osservatorio Astronomico di Capodimonte, Napoli, Italy, <sup>3</sup>INAF - Istituto di Astrofisica e Planetologia Spaziali, Roma, Italy, <sup>4</sup>Landessternwarte Königstuhl Heidelberg, Germany.

We present results, recently published in [5] and based on FLAMES/UVES and FLAMES/GIRAFFE new spectroscopic observations, complemented with FORS2 and VIMOS spectroscopy taken from the literature, of young stellar objects (YSOs) in the L1615/L1616 star-forming region [9]. Our final sample consists of 54 objects with masses  $M_\star \sim 0.1 - 2.3 M_\odot$ .

L1615/L1616, at a distance of about 450 pc [14], is a small Orion outlying cometary cloud [2] in which there is evidence of ongoing star formation activity maybe triggered by the UV radiation coming from massive stars in the Orion OB association [13,3].

As a continuation of previous works performed by [3] and [8], mainly focused on the investigation of the star formation history, the relevance of the triggered scenario, and the study of initial mass function, here we used optical spectroscopy to address the accretion properties of the YSOs in the cloud. In particular, we considered the luminosity of five emission lines ( $H\alpha$ ,  $H\beta$ ,  $\text{He I } \lambda 5876 \text{ \AA}$ ,  $\text{He I } \lambda 6678 \text{ \AA}$ , and  $\text{He I } \lambda 7065 \text{ \AA}$ ) to estimate the mass accretion rates ( $\dot{M}_{acc}$ ) and investigate possible correlation with stellar and infrared properties.

Our main results can be summarized as follows:

1. The YSOs in L1615/L1616 observed with FLAMES show a distribution in radial velocity peaked at  $V_{rad} = 23.2 \pm 3.1 \text{ km s}^{-1}$  and a mean lithium abundance of  $\log n(Li) = 3.3 \pm 0.3 \text{ dex}$ . This confirms their membership to the cometary cloud and their youth.
2. The fraction of accretors in L1615/L1616 we estimated through the criteria by [15] is close to 30%. This percentage is consistent with the fraction of disks reported by [12] for an age of  $\sim 3 \text{ Myr}$ .
3. The  $\dot{M}_{acc}$  derived through secondary diagnostics (in the range  $\sim 10^{-10} - 10^{-7} M_\odot \text{ yr}^{-1}$ ) and the accretion properties of the YSOs in L1615/L1616 are similar to those of other star-forming regions, like Lupus or Taurus. This might imply that environmental conditions to which the cometary cloud is exposed do not influence the accretion evolution of the YSOs within the cloud.
4. Different methods and evolutionary tracks used to derive stellar parameters and mass accretion rates introduce dispersion in the  $\dot{M}_{acc} - M_\star$  relation (see Fig. 1), as recently found by other authors.
5. As in previous studies, strong accretors (i.e., those with  $\log \dot{M}_{acc} \gtrsim -8.5 \text{ dex}$ ) show large excesses in the  $JHKs$  bands, indicative of inner optically thick disk.

## References.

[1] Alcalá et al. 2014 A&A, 561, 2

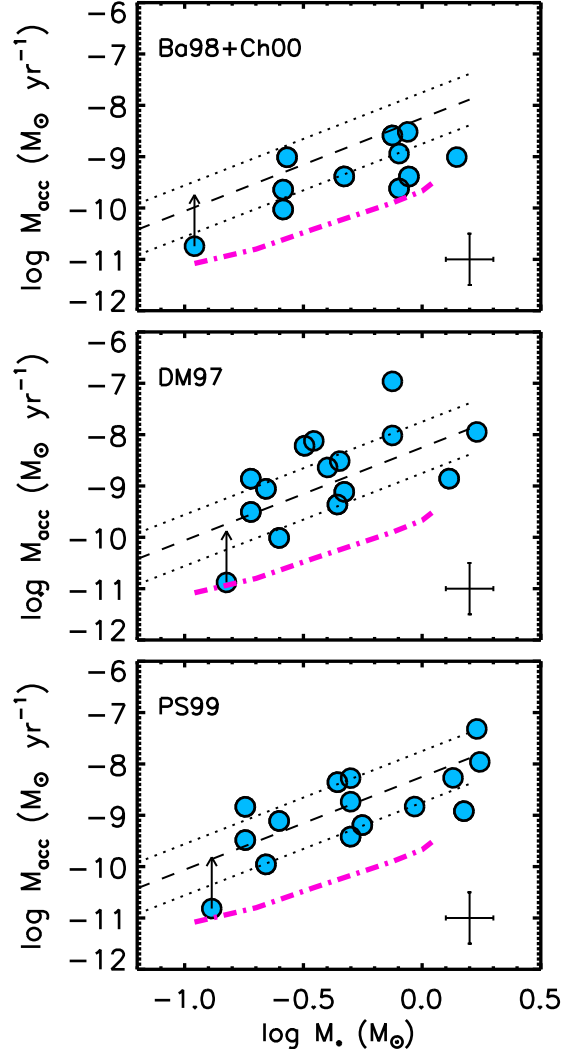


Figure 1:  $\dot{M}_{acc}$  versus  $M_\star$  obtained from [4,6], [7], and [11] tracks, respectively, from the top to the bottom panel. Dashed and dotted lines represent the  $\dot{M}_{acc} - M_\star$  relation and the  $1\sigma$  deviation obtained by [1] in Lupus. The vertical arrow shows the position of a subluminoous object we found in the sample and after applying the correction described in [5]. The dash-dotted line represents the boundary at 3 Myr due to chromospheric activity [10]. Mean error bars are overlaid on the lower-right corner of each panel.

[2] Alcalá, J. M., Covino, E., & Leccia, S. 2008, in *Handbook of Star Forming Regions*, Vol. I: The Northern Sky ASP

Monograph Publications, Vol. 4, ed. B. Reipurth, 801

- [3] Alcalá, J. M., Wachter, S., Covino, E., et al. 2004, *A&A*, 416, 677
- [4] Baraffe, I., & Chabrier, G. 2010, *A&A*, 521, 44
- [5] Biazzo, K., Alcalá, J. M., Frasca, A., et al. 2014, *A&A*, 572, A84
- [6] Chabrier, G., Baraffe, I., Allard, F., & Hauschildt, P. H. 2000, *A&A*, 342, 464
- [7] D'Antona, F., & Mazzitelli, I. 1997, *MSAIt*, 68, 807
- [8] Gandolfi, D., Alcalá, J. M., Leccia, S., et al. 2008, *ApJ*, 687, 1303
- [9] Lynds, B. T. 1962, *ApJS*, 7, 1
- [10] Manara, C. F., Testi, L., Rigliaco, E., et al. 2013, *A&A*, 551, A107
- [11] Palla, F., & Stahler, S. W. 1999, *ApJ*, 525, 772
- [12] Ribas, A., Merín, B., Bouy, H., Maud, L. T. 2014, *A&A*, 561, 54
- [13] Stanke, R., Smith, M. D., Gredel, R., & Szokoly, G. 2002, *ApJ*, 393, 251
- [14] Warren, W. H. Jr., & Hesser, J. E. 1978, *ApJS*, 36, 497
- [15] White, R. J., & Basri, G. 2003, *ApJ*, 582, 1109

## MASS ACCRETION IN PRE-MAIN-SEQUENCE STARS: THE CORE STRIKES BACK

D. Fedele<sup>1</sup>, C. F. Manara<sup>2</sup>; <sup>1</sup>*Max Planck Institut für Extraterrestrische Physik, Garching bei München, Germany*, <sup>2</sup>*ESA/ESTEC, Noordwijk, The Netherlands*.

The mass accretion process in pre-main-sequence stars is one of the main processes that govern the dissipation timescale of gas in disks. Accretion produces a strong and energetic radiation field that regulates the gas temperature and thus it also controls the chemical evolution of the disk. Despite its importance, our understanding of the mass accretion process is still largely incomplete. In particular, early measurements of the mass accretion rate showed a large scatter of the rate of mass accretion for a given stellar mass (e.g., [1]). This implies that viscous evolution and mass accretion are controlled not only by the central star. Note however that part of the scatter in the  $\dot{M}_{acc} - M_*$  is due to observational uncertainties.

The most direct tool of investigation of mass accretion is the measurement of the Balmer continuum produced at the base of the accretion shock. The Balmer continuum emission in excess to the stellar photospheric emission can be then converted to an accretion luminosity and finally to the mass accretion rate. This requires the knowledge of the stellar properties (e.g., mass, temperature, radius) and of the interstellar extinction. To reduce the observational uncertainties is important to cover simultaneously a wide wavelength range. This is possible with, e.g., X-Shooter at the VLT (ESO, Chile), that offers medium resolution spectroscopy ( $R \sim 10000 - 15000$ ) from the atmospheric UV edge to the K-band in the near-infrared.

Using X-Shooter, we performed a survey of the pre-main-sequence stars in the Chamaeleon I star forming region. The sample is made of 39 targets, including binaries with spectral type between early-K and late-M. Stellar properties, interstellar extinction and accretion luminosity are measured following the method described in [2]. Figure 1 shows the  $\dot{M}_{acc} - M_*$  diagram. For comparison, we also plot the measurements for the PMSs in Lupus by [3], obtained and analyzed in a similar fashion. As can be seen there is a systematic difference between Lupus and Cha I: the Lupus PMSs show a rather tight correlation between mass accretion rate and stellar mass while the scatter is much larger for the Cha I stars. Note in particular that: 1) Cha I hosts many more strongly accreting objects compared to Lupus and 2) the scatter in the  $\dot{M}_{acc} - M_*$  for Cha I seems to increase with the stellar mass.

The comparison of the Lupus and Cha I X-Shooter dataset suggests that the mass accretion properties of the two regions are different. Observational uncertainties can be ruled out as both dataset are taken with the same instrumental setup and analyzed with the same method. What is the origin of the different spread in the  $\dot{M}_{acc} - M_*$  diagram between Lupus and Cha I? The two regions have slightly different ages and because of viscous evolution the mass accretion rates may differ between the two. We note however that the age difference is too

small compared to the time needed for the viscous evolution to produce detectable variation [4]. A possible explanation can be the initial conditions of the cloud as suggested by [5]. They proposed a scenario in which the scatter in the  $\dot{M}_{acc} - M_*$  diagram reflects the spread of the angular momentum at the beginning of the collapse of the molecular cloud. Complete samples in both star forming regions will allow us to definitely confirm the existence and determine the origin of the different observed  $\dot{M}_{acc} - M_*$  relations.

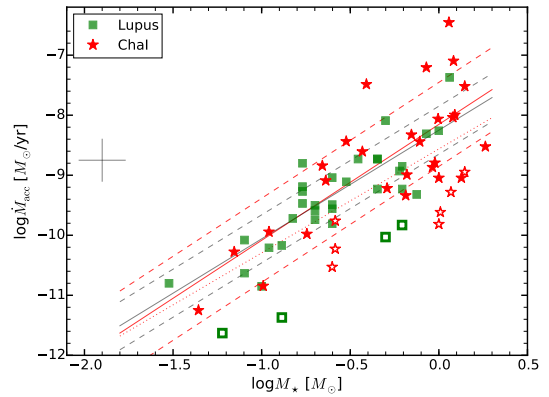


Figure 1: Mass accretion rates vs stellar mass determined from X-Shooter spectra for the sample of young stellar objects in the Chamaeleon I star forming region (red stars) and compared with the values for a sample in Lupus [3]. The best fit relation and its dispersion is shown for the Chamaeleon I objects with a red line and the red dashed lines, while the same is shown with black lines for the Lupus sample. Empty symbols are used for underluminous or non-accreting targets. Adapted from [6].

### References.

- [1] Gullbring, E., Hartmann, L., Briceno, C., & Calvet, N. 1998, *ApJ*, 492, 323
- [2] Manara, C. F., Beccari, G., Da Rio, N., et al. 2013b, *A&A*, 558, A114
- [3] Alcalá, J. M., Natta, A., Manara, C. F., et al. 2014, *A&A*, 561, A2
- [4] Manara, C. F., PhD Thesis, LMU Munich, 2014
- [5] Dullemond, C. P., Natta, A., & Testi, L. 2006, *ApJ*, 645, L69
- [6] Manara, C. F., Fedele, D., & Herczeg, G. in prep.

## A STUDY OF YOUNG STELLAR OBJECTS IN THE $\gamma$ VELORUM AND CHA I CLUSTERS

A. Frasca; *INAF - Osservatorio Astrofisico di Catania, Italy.*

I present here a comparative study of the main properties of the young stellar objects (YSOs) belonging to  $\gamma$  Velorum ( $\gamma$  Vel) and Chamaeleon I (Cha I) clusters/associations, focusing on their rotation, chromospheric radiative losses, and accretion. All these quantities are strongly related to the stellar mass and the evolutionary status.

$\gamma$  Vel (*age*  $\sim 5$ – $10$  Myr) and Cha I (*age*  $\sim 2$  Myr) are the first two young clusters observed in the framework of the Gaia-ESO Survey (GES), a large public spectroscopic survey aimed at the observation of  $\sim 10^5$  stars with the FLAMES multi-object spectrograph at the VLT/UT2 telescope [1].

In this work I used the fundamental parameters (effective temperature, surface gravity, lithium abundance, and radial velocity) delivered by the GES consortium in the first internal data release to select the members of  $\gamma$  Vel and Cha I among the UVES and GIRAFFE spectroscopic observations. A total of 140  $\gamma$  Vel members and 74 Cha I members were studied. The procedures that I developed for the GES analysis node of Catania Observatory to derive stellar fundamental parameters provided also measures of the projected rotational velocity ( $v \sin i$ ) and of the veiling ( $r$ ). Stellar luminosities ( $L_*$ ) and masses ( $M_*$ ) have been derived from spectral energy distributions and by the comparison with evolutionary tracks in the HR diagram. The equivalent widths (EWs) and the fluxes of the  $H\alpha$  and  $H\beta$  lines were measured thanks to the spectral subtraction of low-activity and slowly rotating templates, which are rotationally broadened to match the  $v \sin i$  of the targets. The  $H\alpha$  line was also used for identifying accreting objects, on the basis of its equivalent width and the width at the 10% of the line peak (10% $W$ ), and for evaluating the mass accretion rate ( $\dot{M}_{acc}$ ).

The distribution of  $v \sin i$  for the YSOs of  $\gamma$  Vel is peaked at about  $10 \text{ km s}^{-1}$  and shows a tail toward faster rotators. This suggests the presence of both slowly-rotating stars that are still disk-locked or just decoupled from their disks, and others that have started to spin-up during the phase of contraction and approach to the ZAMS. There is also some indication of a different  $v \sin i$  distribution for the members of its two kinematical populations identified by [2]. A similar distribution, but with a narrower peak, is observed in Cha I. The lower fraction of fast rotators is likely related to the younger age of Cha I.

However, the most striking difference between the YSOs in  $\gamma$  Vel and Cha I is found in the behaviour of the  $H\alpha$  line. Only a handful of stars in  $\gamma$  Vel (about 4% of the members) display signatures of accretion, while many more accretors ( $\sim 40\%$ ) were detected in the younger Cha I, where the highest  $H\alpha$  fluxes are mostly due to accretion, rather than to chromospheric activity.

Accreting and active stars occupy two different regions in a  $T_{eff}$ – $F_{H\alpha}/F_{bol}$  diagram, as shown in Fig. 1, where a simple dividing line has been adopted to distinguish the regime of  $H\alpha$  fluxes dominated by chromospheric emission from that where the accretion is dominant. Further details can be found in [3].

All the non-accreting stars cooler than about 4500–5000 K are very close to the saturation of magnetic activity, as also indicated by the absence of correlation between the  $H\alpha$  flux and  $v \sin i$ . There is a weak tendency of a decrease of flux with increasing temperature for  $T_{eff} > 5000$  K, which is confirmed by the preliminary analysis of GES data of older clusters such as IC 4665 (*age*  $\sim 30$  Myr) and NGC 2547 (*age*  $\sim 35$  Myr).

We derive  $\dot{M}_{acc}$  values in the ranges  $10^{-11}$ – $10^{-9} M_\odot \text{ yr}^{-1}$  and  $10^{-10}$ – $10^{-7} M_\odot \text{ yr}^{-1}$  for  $\gamma$  Vel and Cha I accretors, respectively. We find less scatter in the  $\dot{M}_{acc} - M_*$  relation derived through the  $H\alpha$  EWs, compared to the  $H\alpha$  10% $W$  diagnostics, in agreement with other authors. However, the  $H\alpha$  10% width represents a fast and efficient criterion to select accretor candidates for a deeper analysis.

Moreover, although a wide range of  $\dot{M}_{acc}$  values is observed for the objects with a negligible veiling ( $r < 0.25$ ), all the stars for which we found a veiling greater than 0.25 are accretors. Furthermore, the mass accretion rate displays some correlation with the veiling (see Fig. 2). A Spearman's rank correlation analysis [4] gives a coefficient  $\rho = 0.28$  with a significance of its deviation from zero  $\sigma = 0.10$ , which indicates a marginal correlation. If we limit the analysis to the objects with a significant veiling ( $r \geq 0.25$ ), the degree of correlation is enhanced, as indicated by the values of  $\rho = 0.62$  and  $\sigma = 0.001$ .

This work shows the huge potential of the GES for the study of rotation, activity, and accretion of YSOs in young clusters. This study will be extended to all the pre-main sequence clusters that are being observed by the GES.

### References.

- [1] Gilmore, G., Randich, S., Asplund, M., et al. 2012, *The Messenger*, 147, 25
- [2] Jeffries, R. D., Jackson R. J., Cottaar M., et al. 2014, *A&A*, 563, A94
- [3] Frasca, A., Biazzo, K., Lanzafame, A. C., et al. 2015, *A&A*, 575, A4
- [4] Press, W. H., Teukolsky, S. A., Wetterling, W. T., & Flannery, B. P. 1992, *Numerical Recipes, The Art of Scientific Computing* (Cambridge University Press), second edition

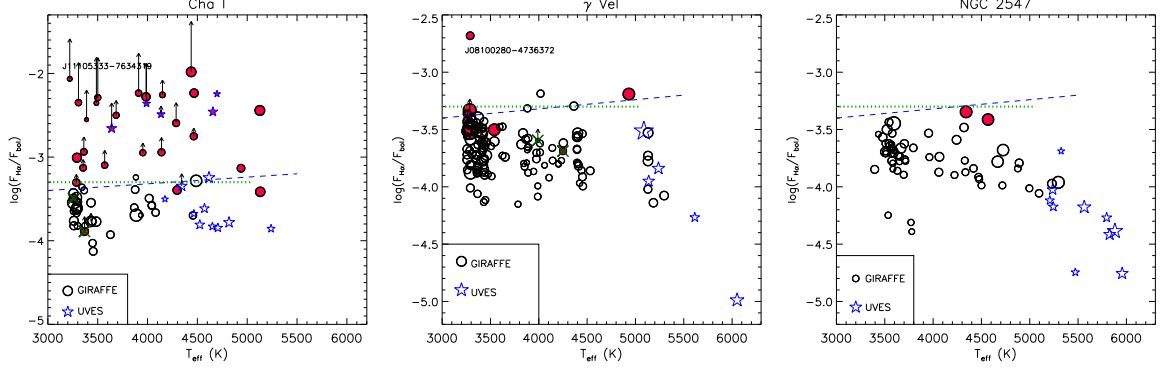


Figure 1:  $H\alpha$  flux (in units of the bolometric flux) versus  $T_{eff}$  for the members of Cha I (left panel),  $\gamma$  Vel (middle panel), and NGC 2547 (right panel) clusters. The symbol size scales with the  $v \sin i$ . Filled symbols denote the accretor candidates ( $10\% W_{H\alpha} > 270 \text{ km s}^{-1}$ ). The flux values corrected for veiling by the factor  $(1 + r)$  are denoted by arrowheads. In each box, the dashed straight line is drawn to follow the upper envelope of the sources without accretion and is very close to the saturation of chromospheric activity (dotted line).

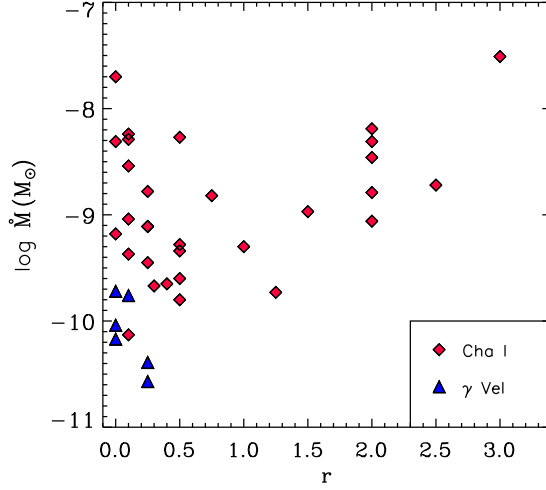


Figure 2: Mass accretion rate from  $EW_{H\alpha}$  versus veiling. Diamonds and triangles represent Cha I and  $\gamma$  Vel stars, respectively.

## EXORCISM: EXOR OPTICAL-INFRARED SYSTEMATIC MONITORING

T. Giannini; *INAF - Osservatorio Astronomico di Roma, Monte Porzio Catone, Italy.*

EXORCISM is the long-term optical-infrared monitoring of EXors, a class of Pre-main Sequence stars undergoing intermittent outbursts (with timescales of tens of years and duration of about one year) with typical amplitudes 2-5 magnitudes in the visual band (see e.g. [1]). These bursts are usually interpreted as due to episodic accretion events; nevertheless several fundamental aspects of the EXor phenomenon are still very poorly known: 1) are EXors peculiar objects or rather they represent a short but common and repetitive phase of the pre-main evolution? 2) which is the mechanism at the origin of the burst (disk thermal or gravitational instability, perturbation of the disk induced by an external body?) 3) which is the role of the episodic accretion in disk fragmentation and evolution? 4) are EXors distinct objects from FUors (pre-main sequence objects with stronger bursts with longer duration) or rather they represent the same phenomenon in a subsequent evolutionary phase?

From an observational point of view the poor knowledge of the EXors behavior is mainly due to a lack of long-term multi-wavelength monitoring programs aiming at studying the photometric and spectroscopic properties. Moreover, only few studies exist that compare photometry and/or spectroscopy of the outburst and quiescence phase ([2],[3],[4]) and observations at high angular resolution to spatially resolve the inner disk.

Our monitoring envisages to perform on monthly basis optical and near-infrared photometry of all the known EXors and candidates (around 30 objects). In addition, optical-infrared spectroscopy is performed roughly every year. Prompt detection and follow-up of any burst is also planned. The facilities routinely involved in the program are : AZT24 at Campo Imperatore (Italy) for near-infrared imaging and spectroscopy of northern objects; REM at ESO-La Silla for optical-infrared imaging of southern objects; LX200 at St. Petersburg University for optical imaging. In addition, several focussed programs are on-going at TNG and NOT (Canary Islands), and LBT (Tucson) essentially to perform deep optical-infrared spectroscopy (Fig. 1). EXORCISM have so far produced a number of papers, to which we refer as far as the main results of our

study are concerned ([5]-[18]).

### References.

- [1] Miller, A. A., Hillenbrand, L. A., Covey, K. R., et al. 2011, *ApJ*, 730, 80
- [2] Sipos, N., Ábrahám, P., Acosta-Pulido, J., et al. 2009, *A&A*, 507, 881
- [3] Sicilia-Aguilar, A., Kóspál, Á., Setiawan, J., et al. 2012, *A&A*, 544, A93
- [4] Juhász, A., Dullemond, C. P., van Boekel, R., et al. 2012, *ApJ*, 744, 118
- [5] Lorenzetti, D., Giannini, T., Calzoletti, L., et al. 2006 *A&A*, 453, 579
- [6] Lorenzetti, D., Giannini, T., Larionov, V.M., et al. 2007 *ApJ*, 665, 1182
- [7] Lorenzetti, D., Larionov, V.M., Giannini, T., et al. 2009, *ApJ*, 693, 1056
- [8] Giannini, T., Lorenzetti, D., Elia, D., et al. 2009, *ApJ*, 704, 606
- [9] Lorenzetti, D., Giannini, T., Larionov, V.M., et al. 2011 *ApJ*, 732, 69
- [10] Lorenzetti, D., Antonucci, S., Giannini, T., et al. 2012 *ApJ*, 749, 188
- [11] Lorenzetti, D., Antonucci, S., Giannini, T., et al. 2013 *ApSS*, 343, 535
- [12] Antonucci, S., Giannini, T., Lorenzetti, D. 2013 *New Astronomy*, 98, 106
- [13] Antonucci, S., Giannini, T., Li Causi, G. et al 2014 *ApJ*, 782, 51
- [14] Lorenzetti, D., Antonucci, S., Giannini, T., et al. 2014 *ApSS*, 353, 567
- [15] Antonucci, S., Arkharov, A.A., Di Paola, A. et al 2014 *A&A*, 575, L7
- [16] Giannini, T., Lorenzetti, D., Antonucci, S., et al. 2014 *ApSS*, 352, 691
- [17] Lorenzetti, D., Antonucci, S., Giannini, T., et al. 2015, *ApJ*, 802, 24
- [18] Antonucci, S., Nucita, A., Giannini, T., et al. 2015 *A&A*, submitted

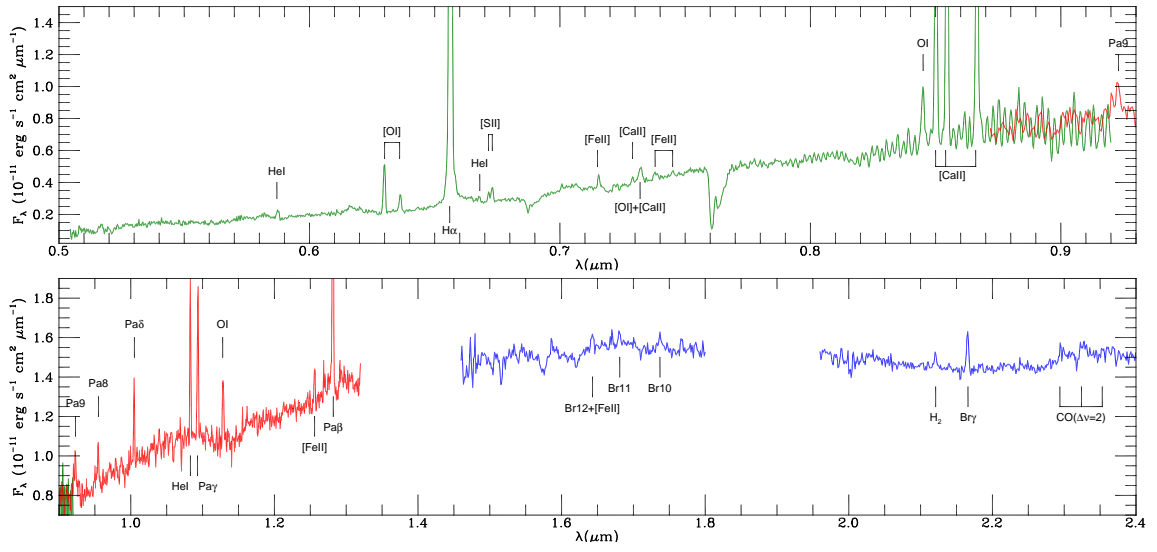


Figure 1: Optical (LBT-MODS) and near-infrared (TNG-NICS) spectrum of V1118 Ori during a quiescent phase.

## ACCRETION AND WIND PROXIES THROUGHOUT DISK EVOLUTION

C.F. Manara; *ESA/ESTEC, Noordwijk, The Netherlands.*

The evolution of protoplanetary disk and their ability to form planets is strictly related to the distribution and the amount of gas in the disk [1]. This can directly be traced in the outer disk through observations of molecular gas emission lines at various wavelengths, e.g., in the sub-mm [2]. On the other hand, the interaction of the disk with the central star through accretion of matter allows us to access observationally to the gas content in the innermost region of the disk, at distances as close to the star as  $\sim 0.1$  AU [3]. Similarly, studies of the wind properties of young stellar objects (YSOs) help us in constraining the properties of the gas in the inner part of the disk [4] and the mechanisms that lead to the final disk dispersal [5]. Here I report on recent work carried out with various members of the Jets and Disks at INAF (JEDI) collaboration to study protoplanetary disk evolution through the analysis of accretion and wind properties of YSOs in various star-forming regions and at different stages of disk evolution.

The data presented in this contribution have been obtained with the VLT/X-Shooter spectrograph, that covers simultaneously and with medium resolution the range of wavelengths  $\lambda \sim 300$ -2500 nm. Therefore, spectra obtained with this instrument allow us to access the most direct proxy of accretion, that is the UV-excess shortward the Balmer jump, several permitted emission lines (e.g.,  $H\alpha$ ,  $H\beta$ ,  $CaH$ ,  $CaK$ ,  $Pa\beta$ ,  $Br\gamma$  [6]) and forbidden lines (e.g.,  $[OI]\lambda 6300$  Å [4]), and also several photospheric absorption features (e.g., Li). We have recently developed an automatic procedure to determine from such spectra the stellar and accretion parameters of YSOs [7]. We find the best fit in a grid of models that includes various photospheric templates, mostly from [8], a set of slab model to reproduce the excess emission due to accretion, and a reddening law to take into account the effects of interstellar absorption (Fig. 1). This method has already been applied to a large number of YSOs in the Lupus region [6], where we have found that the scatter of the mass accretion rates ( $\dot{M}_{acc}$ ) at any given stellar mass ( $M_*$ ) is significantly smaller than in previous works. We have also used this method to study a sample of 22 transition disks (TDs) [9]. Our study has shown that there are (at least) some TDs with  $\dot{M}_{acc}$  as high as those of full disks, a finding difficult to be explained by current models. Indeed, this suggest that the innermost region of their disk, although dust depleted, is significantly gas rich in order to sustain the observed  $\dot{M}_{acc}$ . Similarly, we have found that the winds traced by the  $[OI]\lambda 6300$  Å line scale with the accretion rates in the same fashion as in full disks. This line could trace gas from a large region in the disk [10], and we are now carrying out further studies with higher resolution spectra to understand whether this is valid also in TDs, and what kind of wind is this line actually tracing [11].

To further constrain the evolution of protoplanetary disks is important to study objects with different intrinsic properties, such as age,  $M_*$ , or the environment in which they are

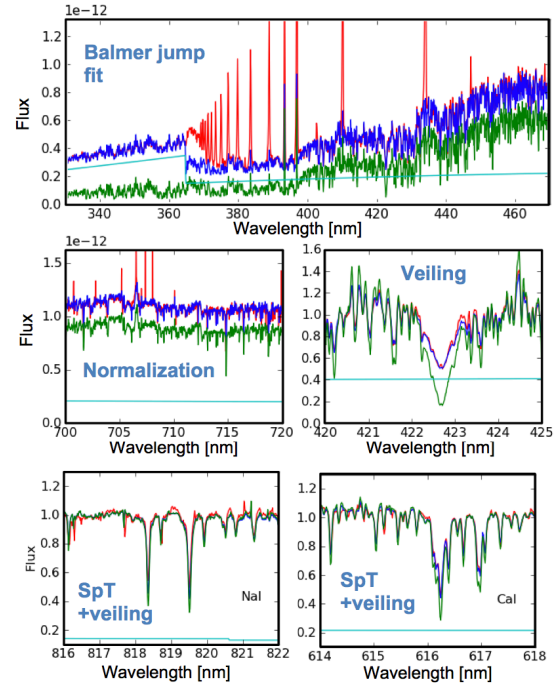


Figure 1: Example of best-fit of X-Shooter spectra using the procedure described in [7]. The observed spectrum is shown in red, the best fit in blue, the reddened photospheric template in green and the slab model spectrum in cyan.

located. With the JEDI collaboration we have studied eight very low-mass objects in the  $\sim 3$ -5 Myr old  $\sigma$ -Orionis cluster [12], 36 YSOs in the  $\sim 2$ -3 Myr old Lupus region [6], and some objects in the old ( $\sim 5$ -10 Myr) TWA association [13]. Two more samples have now been added to this collection. Here I briefly report the results on the sample of 17 very low-mass YSOs and brown dwarfs (BDs) located in the young ( $\sim 1$  Myr)  $\rho$ -Ophiucus cluster [14], while in the contribution by Fedele we report on the sample of 31 YSOs in the  $\sim 2$ -3 Myr old Chamaeleon I region [15]. Studying YSOs located in the  $\rho$ -Ophiucus cluster is more challenging than studying objects in other older and less embedded region. Indeed, the extinction towards a single target in  $\rho$ -Ophiucus can be as high as  $A_V \sim 10$ -15 mag, or even more. Therefore, none of the X-Shooter spectra we obtained had enough S/N in the Balmer continuum to perform the detailed analysis described earlier. We then obtained the stellar parameters (spectral type,  $A_V$ ) by finding the best match between the observed spectrum and a set of reddened photospheric templates, again mostly from [8] or from synthetic spectra. Then, we determined the accretion rates from the intensity of various emission lines. Fig. 2 shows

the values of  $\dot{M}_{acc}$  vs  $M_*$  for the objects analyzed in this study and for the Lupus and  $\sigma$ -Orionis samples. The best-fit  $\dot{M}_{acc}$ - $M_*$  relation of the Lupus sample is also shown, and it is clear that most of the  $\rho$ -Ophiucus objects follow that same relation. This suggests that this relation holds in the very low-mass and BD range, as well. Moreover, also the values of  $\dot{M}_{acc}$  for  $\rho$ -Ophiucus targets seem to have a similar small scatter around the best-fit relation as the Lupus objects. It is possible that this scatter smaller than in previous works is related to the good quality of the data and the uniform and accurate methodology used in these works. This suggests that larger studies of unbiased samples based on similar data and analyzed with our methodology will really help us in determining the main properties of the accretion process, and thus of the properties of gas in the innermost part of protoplanetary disks as a function of  $M_*$  and age.

We are now collecting a large number of X-Shooter spectra to complete the samples of YSOs with disk in the Lupus and Chamaeleon I regions, and we are asking for similarly complete data-sets in the  $\sigma$ -Orionis, Upper Sco, and  $\rho$ -Ophiucus regions. This will allow us to cover a large range of  $M_*$  and age. All these spectroscopic surveys are coupled with ongoing or future ALMA surveys aimed at determining the outer disk properties. We thus have now a detailed method available to determine stellar and accretion properties of YSOs, we are now working on determining what kind of wind is traced by the forbidden emission lines, and we will then be able few months from now to clearly constrain these processes on large samples of objects with well determined outer disk properties.

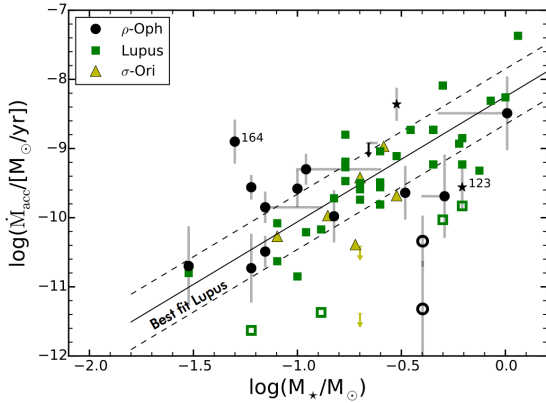


Figure 2: Mass accretion rates vs stellar mass for a sample of very low-mass stars and brown dwarfs in the  $\rho$ -Ophiucus cluster [14], together with objects in the Lupus region [6] and in the  $\sigma$ -Orionis cluster [12]. The best fit relation for the Lupus sample alone and its scatter is also shown. Adapted from [14].

## References.

- [1] Mordasini, C.; Alibert, Y.; Benz, W., et al. 2012, A&A, 541, 97
- [2] Dutrey, A., Semenov, D., Chapillon, E., et al. 2014, Protostars and Planets VI, 317
- [3] Hartmann, L., Calvet, N., Gullbring, E., & Dâ^Alessio, P. 1998, ApJ, 495, 385
- [4] Natta, A., Testi, L., Alcalá, J. M., et al. 2014, A&A, 569, AA5
- [5] Alexander, R., Pascucci, I., Andrews, S., Armitage, P., & Cieza, L. 2014, Protostars and Planets VI, 475
- [6] Alcalá, J. M., Natta, A., Manara, C. F., et al. 2014, A&A, 561, A2
- [7] Manara, C. F., Beccari, G., Da Rio, N., et al. 2013b, A&A, 558, A114
- [8] Manara, C. F., Testi, L., Rigliaco, E., et al. 2013a, A&A, 551, A107
- [9] Manara, C. F., Testi, L., Natta, A., et al. 2014, A&A, 568, AA18
- [10] Rigliaco, E., Pascucci, I., Gorti, U., Edwards, S., & Hollenbach, D. 2013, ApJ, 772, 60
- [11] Manara, C.F., Natta, A., Rigliaco, E. et al. in prep.
- [12] Rigliaco, E., Natta, A., Testi, L., et al. 2012, A&A, 548, A56
- [13] Stelzer, B. et al. in prep.
- [14] Manara, C. F., Testi, L., Natta, A., & Alcalá, J. M. 2015, arXiv:1505.04046
- [15] Manara, C. F., Fedele, D., & Herczeg, G. in prep.

# INVESTIGATING MID-INFRARED HYDROGEN LINES AS ACCRETION INDICATORS

E. Rigliaco; *Department of Physics - Institute for Astronomy, ETH Zurich, Switzerland.*

I summarize here the properties of the Hydrogen recombination lines observed in the mid-infrared (mid-IR) *Spitzer* spectra of disk-bearing objects [9]. In particular, I investigate their nature as accretion indicators, and the possibility of using these lines to measure accretion in embedded class-I objects where optical tracers cannot be used.

A quantitative estimate of the accretion of mass from the circumstellar disk onto central star in young stellar objects (YSOs) can be measured using several indicators. In the past few years many works have in fact shown that many emission lines observed in YSOs' spectra (mainly hydrogen recombination lines) are correlated with the accretion luminosity ( $L_{acc}$ , [3,7,4,5,8,2,1], among others). Even if these accretion indicators span over a huge range of wavelengths, from the near-ultraviolet to the near-infrared, they cannot be used to measure accretion in embedded objects, where the UV and optical radiation is absorbed by the remnant infall envelope and re-emitted at longer wavelengths.

In [9] we focused on the strongest of the Humphreys Series lines in the mid-IR, the  $Hu\alpha$  at  $12.37\mu\text{m}$  (hereafter  $H\text{I}(7-6)$ ) and the  $H\text{I}(9-7)$  line at  $11.31\mu\text{m}$ , both observed with the InfraRed Spectrograph (IRS) on the *Spitzer* Space Telescope, aiming at unveiling their nature as accretion indicators.

We analyzed a sample of  $\sim 100$  disk-bearing objects collected from the *Spitzer* Archive in different evolutionary stages: from full to transitional and debris disks. We measured the  $H\text{I}$  line luminosities, and the hydrogen line ratios.

We found that full and transitional disks show a correlation between the  $H\text{I}$  line luminosity and  $L_{acc}$  [9]:

$$\begin{aligned} \text{Log}(L_{H\text{I}(7-6)}/L_{\odot}) = \\ = (0.48 \pm 0.09) \times \text{Log}(L_{acc}/L_{\odot}) - (4.68 \pm 0.10) \end{aligned} \quad (1)$$

The same correlation cannot be tested against debris disks since no information about the accretion luminosity can be retrieved due to their more advanced evolutionary stage. Moreover, we found that the physical properties of the emitting gas, obtained through the  $H\text{I}(7-6)/H\text{I}(9-7)$  line ratio are fairly well constrained using the prediction of the theoretical models by [6] that replicate the conditions in the region of winds and accretion flows in accreting YSOs. These two results suggest that the  $H\text{I}$  mid-infrared lines observed in full and transitional are likely accretion indicators as the other hydrogen recombination lines at shorter wavelengths.

Interestingly,  $H\text{I}(7-6)$  emission is also observed in a sample of debris disks. A chromospheric origin of these lines

seems likely, but it is not possible to definitively rule out either a long-lasting accretion signature nature or the presence of a non-resolved accreting companion. If we assume the same correlation in Eq. 1 can be used for debris disks, we find that the observed  $H\text{I}$  lines would trace accretion luminosities as low as  $< 10^{-10} M_{\odot}/\text{yr}$ . Optical and UV accretion diagnostics are not sensitive to such low mass accretion rates for Sun-like stars.

The analysis of archival *Spitzer* spectra of disk-bearing objects has highlighted two main aspects that deserve to be better investigated in the future:

- the presence of mid-IR hydrogen recombination lines in debris disks;
- the possibility of using these line luminosities to determine the accretion rates in still embedded class I objects.

Although in class I objects the obscuration of the protostar by the envelope and disk is significant ( $A_V=10-50$  mag), it can still be detected at infrared wavelengths. Estimating the infall accretion in class I objects will certainly help to better understand the earlier stages of stellar evolution, and within the JETS and DISKS INAF projects it will help to link the studies of pre-stellar cores and molecular jets to the accretion properties of more evolved class II objects.

## References.

- [1] Alcalà, J. M., Natta, A., Manara, C., et al. 2014, A&A, 561, 2A
- [2] Antonucci, S., García-López, R., Nisini, B., et al. 2014, A&A, 572A, 62A
- [3] Gullbring, E., Hartmann, L., Briceño, C., & Calvet, N. 1998, ApJ, 492, 323G
- [4] Herczeg, G. & Hillenbrand, L. 2008, ApJ, 681, 594H
- [5] Ingleby, L., Calvet, N., Bergin, E. et al. 2011, ApJ, 743, 105I
- [6] Kwan, J., & Fischer, W. 2011, MNRAS, 411, 2383K
- [7] Natta, A., Testi, L. & Randich, S. 2006, A&A, 452, 245N
- [8] Rigliaco, E., Natta, A., Testi, L., et al. 2012, A&A, 548A, 56R
- [9] Rigliaco, E., Pascucci, I., Duchene, G., et al. 2015, ApJ, 801, 31

## **Part 3:**

### ***Jets and Winds***

# EFFECTS OF ASYMMETRIC JETS ON THE DYNAMICS OF PROTOPLANETARY DISKS: STUDY OF A SIMPLE MODEL

F. Bacciotti<sup>1</sup>, U. Locatelli<sup>2</sup>, R.I. Páez<sup>2</sup>, M. Volpi<sup>2</sup>; <sup>1</sup>INAF – Osservatorio Astrofisico di Arcetri, Italy, <sup>2</sup>Dip. di Matematica, Università di Roma “Tor Vergata”.

## 1. Introduction

Extrasolar planets can appear in very different dynamical configurations (see [2]). In particular, the orbits of some multi-planetary systems can show values of the eccentricities much larger than those in our solar system (in which the orbits are nearly circular). This is somewhat surprising, as large eccentricities could prevent the stability of such systems (because close encounters between planets become more likely).

Here we investigate if the orbital properties of the planets can be related to the formation of these systems, and in particular to bipolar collimated outflows of matter (jets), which are ubiquitous around Young Stellar Objects (YSOs). The jet physical properties can be studied using spectroscopic diagnostic techniques (see [1]). In particular, this allows us to measure the flux of linear momentum (hereafter  $\dot{\mathbf{p}}$ ) of the jets in the two lobes, that propagate perpendicularly to the disk midplane. The jet lobes are often asymmetric and are found to have a different linear momentum flux (that is  $\Delta\dot{\mathbf{p}} \neq \mathbf{0}$ ). This produces a feedback on the inner part of the disk, from where the jet is accelerated, because the orbital motion of the matter in this region is influenced by a reaction force  $-\Delta\dot{\mathbf{p}}$  (assumed here to be perfectly vertical with respect to the disk midplane).

In the present work, we want to describe the first steps of an ambitious project willing to link the two topics introduced above. In particular, we want investigate if the described jet feedback excites the eccentricities of the orbital motions up to the values observed in extrasolar systems. Said in other words, are the orbital properties of the currently observed exoplanets a legacy of the primordial formation mechanism?

Some of these ideas have been investigated in the past by Namouni (see [7] and the references therein). However, in our model we remove some inconsistencies of that approach. In particular we do not consider already formed (proto)planets, which begin to exist close to the end of the estimated lifetime of jets, i.e.  $10^6$  yrs (see [3]). Moreover, differently by [7], we do not model the feedback  $-\Delta\dot{\mathbf{p}}$  as due to an asymmetric stellar wind, but we assume it is due to a disk wind (which has a much larger effect on the system).

## 2. The model and the choice of its parameters

We drastically simplify the problem of the disk dynamics, by making the following assumptions, which are schematically represented in Figure 1: (I) the (proto)star is a point mass; (II) both the inner part of the disk (at the jet base) and the external one (all the rest) are represented by two horizontal non-rigid circular rings of matter; (III) the whole system is axisymmetric with respect to the vertical axis passing through the star and the centers of both rings; (IV) the masses of the star and each ring are constant; (V) masses are homogeneously spread along each ring; (VI) there is a constant upward force

$\mathbf{F} = -\Delta\dot{\mathbf{p}}$  acting on the first ring as a reaction to the launching mechanism producing the two lobes of the jet; (VII) all the forces are neglected except for  $\mathbf{F}$  and the gravitational interactions between the star and each of the two rings, and the rings one with each other.

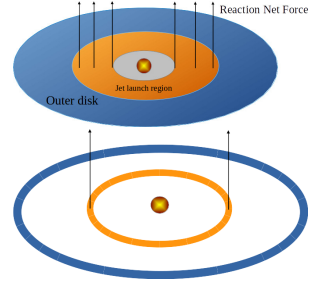


Figure 1: Scheme representing the elements of the model.

We denote with  $R_1$  and  $R_2$  the radii of the two rings, while  $z_0, z_1, z_2, m_0, m_1$  and  $m_2$  are the vertical quota and the masses of the star and the rings, respectively. Let us emphasize that the rings can both pulsate and move vertically, thus,  $R_1, R_2$  and  $z_j$  ( $\forall j = 0, 1, 2$ ) are functions of time  $t$ . Moreover, the evolution of each ring can be described by the motion of a single point belonging to it, because the position of all other points is obtained by suitable axial rotations starting from that point acting as a generic representative of the ring itself. This highlights the fact that our model has nine degrees of freedom (d.o.f.). In order to separate the motion of the barycenter and to suitably use our numerical integrator (see next section), it is convenient to adopt the Jacobi canonical coordinates  $(\tilde{\mathbf{v}}_1, \tilde{\mathbf{v}}_2, \mathbf{v}_1, \mathbf{v}_2)$ . Here  $\mathbf{v}_1$  locates the generic representative of the first ring with respect to the star, while  $\mathbf{v}_2$  is nearly equal to the astrocetric position of the generic representative of the second ring, while  $\tilde{\mathbf{v}}_j$  is the conjugate momentum with respect to  $\mathbf{v}_j$ ,  $\forall j = 1, 2$  (see [4]). Therefore, our model is fully described by the following 6 d.o.f. Hamiltonian:

$$H(\tilde{\mathbf{v}}_1, \tilde{\mathbf{v}}_2, \mathbf{v}_1, \mathbf{v}_2) = A(\tilde{\mathbf{v}}_1, \tilde{\mathbf{v}}_2, \mathbf{v}_1, \mathbf{v}_2) + B(\mathbf{v}_1, \mathbf{v}_2), \quad (1)$$

where the main part  $A = \mathcal{K}_1(\tilde{\mathbf{v}}_1, \mathbf{v}_1) + \mathcal{K}_2(\tilde{\mathbf{v}}_2, \mathbf{v}_2)$  is given by the sum of two separated Keplerian terms, that are

$$K_j(\tilde{\mathbf{v}}_j, \mathbf{v}_j) = \frac{\mu_j \tilde{\mathbf{v}}_j \cdot \tilde{\mathbf{v}}_j}{2\mu_{j-1}m_j} - \frac{G\mu_{j-1}m_j}{\|\mathbf{v}_j\|} \quad \forall j = 1, 2, \quad (2)$$

being  $\mu_0 = m_0$ ,  $\mu_1 = \mu_0 + m_1$  and  $\mu_2 = \mu_1 + m_2$ . In general, the Keplerian part  $A$  is much greater than the purely potential term, which is

$$B = -\frac{Gm_0m_2}{\|\mathbf{v}_2 + \frac{m_1}{\mu_1}\mathbf{v}_1\|} + \frac{G\mu_1m_2}{\|\mathbf{v}_2\|} + V_1 + U_{12}, \quad (3)$$

where both  $V_1$ , that is the potential energy corresponding to the vertical force  $\mathbf{F}$ , and the term due to the gravitational interaction between the rings, i.e.

$$U_{12} = - \int_0^{2\pi} \frac{Gm_1m_2 d\psi}{\sqrt{R_1^2 + 2R_1R_2 \cos \psi + R_2^2}}, \quad (4)$$

must be expressed as functions of the Jacobi variables  $(v_1, v_2)$ .

We fix most of the parameters and the initial conditions as follows. According to the values commonly reported in the scientific literature, we set  $m_1 + m_2 = m_0/100$  and we assume that  $r_0 = 0.01 \text{ AU}$ ,  $r_i = 10 \text{ AU}$ ,  $r_e = 200 \text{ AU}$ , where  $r_0$  and  $r_i$  denote the radii of the circles bounding the internal (orange) jet launch region in the upper part of Figure 1, resp., while  $r_e$  is the outer radius of the disk. The initial value of the radius  $R_1(0)$  is set to be equal to the average distance of the internal part of the disk, while  $R_2(0)$  is fixed so that the gravitational energy due to the interaction between the first ring and the outer disk is exactly equal to the value assumed by  $U_{12}$  in (4), when we put  $R_1 = R_1(0)$  and  $R_2 = R_2(0)$ . In order to perform these calculations, we need to assume a disk density distribution law, that can be found, e.g., in [8]. Moreover, all the initial quotas and vertical velocities are set equal to zero, while the initial angular velocity of the matter in each ring is fixed so that its radius would constant if the other ring and the vertical force  $\mathbf{F}$  are not present. Just two parameters have not yet been fixed: the stellar mass  $m_0$  and  $\mathbf{F} = -\Delta\mathbf{p}$ . We compiled these values for different YSOs using from the recent literature (see Figure 2). We are interested in evaluating the effects induced by the strongest vertical force, and thus we focus on the case of *LkH $\alpha$  233*, where  $m_0 = 2.9 M_\odot$  and  $\|\mathbf{F}\| \simeq 6.4 \times 10^{-6} M_\odot \text{AU}/\text{yr}^2$  (see [6]).

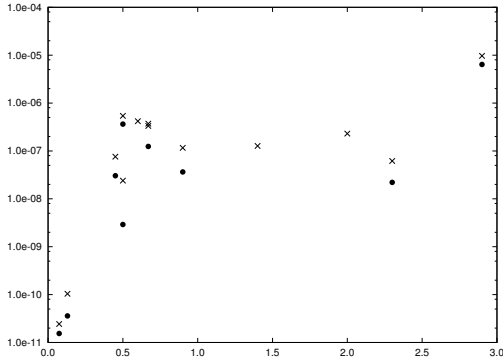


Figure 2:  $\|\mathbf{p}\|$  (symbol:  $\times$ ) on a single lobe of a jet and  $\|\Delta\mathbf{p}\|$  (when data on the two lobes are available, symbol:  $\bullet$ ) as a function of the stellar mass.

### 3. First numerical results and conclusions

In order to numerically integrate the twelve Hamilton equations

$$\frac{d\tilde{v}_j}{dt} = -\nabla_{v_j} H, \quad \frac{d\mathbf{v}_j}{dt} = \nabla_{\mathbf{v}_j} H, \quad \forall j = 1, 2, \quad (5)$$

it is convenient to use the method *SBAB<sub>3</sub>*, belonging to a set of symplectic integrators often used in Celestial Mechanics (see [5]). The tests on the preservation of the energy (as well as many details missing in this short note) are reported in [9].

Despite both rings always remain horizontal and circular, each *generic representative* of a ring moves on an orbit that can be instantaneously approximated with a Keplerian ellipse. Thus, we can numerically compute the evolution (in time) of the value of the eccentricity that is related to each ring. Figure 3 shows the behavior of the eccentricity related to the first ring for a model, having the same values of the parameters reported in the previous section, but the vertical force that is *increased by a factor 100*, i.e., now  $\|\mathbf{F}\| \simeq 6.4 \times 10^{-4} M_\odot \text{AU}/\text{yr}^2$ . In Figure 3, one can appreciate that the average eccentricity is nearly equal to the current value characterizing the Earth orbit.

In conclusion, our first numerical investigations show that the the feedback exerted by asymmetric jets on the disks can effectively increase the eccentricity of orbital motions (initially set to be circular). However, this mechanism looks far from being able to explain the large eccentricities observed in some exoplanetary systems. Possibly this is due to a deficiency of our model. Our next step will be to refine the model by including a much larger number of rings, so to describe a situation closer to a disk with a continuous distribution of matter.

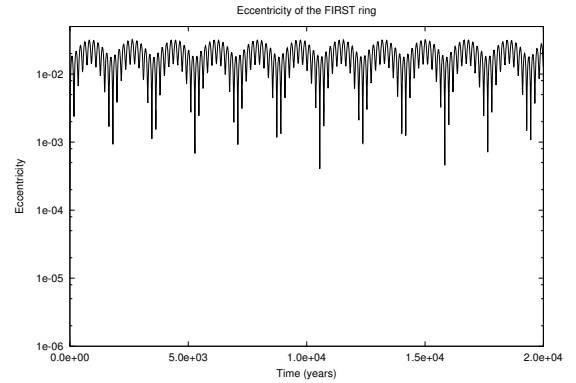


Figure 3: Behavior of the eccentricity related to the first ring.

### References.

- [1] Bacciotti & Eislöffel 1999, *A&A*, 342, 717
- [2] Beaugé et al. 2012, *Res. in Astron. & Astroph.*, 12, 1044.
- [3] Crida 2009, in *Reviews in Modern Astronomy*, 21, 215.
- [4] Laskar 1989, in *Notes Scientifiques et Techniques du Bureau des Longitudes*, #S026.
- [5] Laskar & Robutel 2001, *Cel. Mech. Dyn. Astr.*, 80, 39.
- [6] Melnikov et al. 2008, *A&A*, 483, 199.
- [7] Namouni 2013, *Astroph. & Sp. Sc.*, 343, 53.
- [8] Sheikhnezami et al. 2012, *Astroph. J.*, 757, 65.
- [9] Volpi 2015, Master Thesis in Mathematics.

## SHOCKS IN ACCRETION/EJECTION PROCESSES: OBSERVATIONS, MODELS, AND LABORATORY EXPERIMENTS

R. Bonito<sup>1,2</sup>; <sup>1</sup>*Dipartimento di Fisica e Chimica - Universita' di Palermo, Italy*, <sup>2</sup>*INAF - Osservatorio Astronomico di Palermo, Italy*.

Stellar jets have been observed in a wide range of wavelengths, from radio to optical, and X-rays, showing complex morphologies along the jet axis: chain of knots, bow shocks, as well as stationary and elongated high energy emission mainly detected near the driving source. We developed detailed numerical models to explain the knotty structure detected mainly in the optical [3] and the stationary X-ray emission from the base of stellar jets [4], both considering pulsed jets (with variable initial velocity of ejection) and diamond shocks formed in the nozzle scenario [5]. The model takes into account all the relevant physical processes such as the radiative losses and the thermal conduction which are fundamental to compare the model's predictions with the observations [3]. The emission maps synthesized from the models can be directly compared with the observations performed e.g. with the Hubble Space Telescope in the optical and with Chandra in X-rays ([2,7]; see also Fig. 1).

A new approach is also discussed which takes into account the effects of the magnetic field: a combination of laboratory experiments, numerical models, and comparison with obser-

vations [1]. The opposite process of mass accretion has been also investigated taking advantage of the numerical magnetohydrodynamic simulations and diagnostic tools to compare the spectra with the observations [6]. Future perspectives include the laboratory experiments of accretion shocks and a magnetized jet with the thermal conduction included [8] from which both thermal and non-thermal emission can be synthesized from the models and compared with current multi-wavelength observations (e.g. radio, optical, X-rays).

### References.

- [1] Albertazzi et al. 2014, *Science*, 346, 325
- [2] Bonito et al. 2008, *A&A*, 484, 389B
- [3] Bonito et al. 2010a, *A&A*, 511, A42
- [4] Bonito et al. 2010b, *A&A*, 517, A68
- [5] Bonito et al. 2011, *ApJ*, 737, 54
- [6] Bonito et al. 2014, *ApJ*, 795L, 34B
- [7] Bonito et al. in prep.
- [8] Ustamujic et al. in prep.

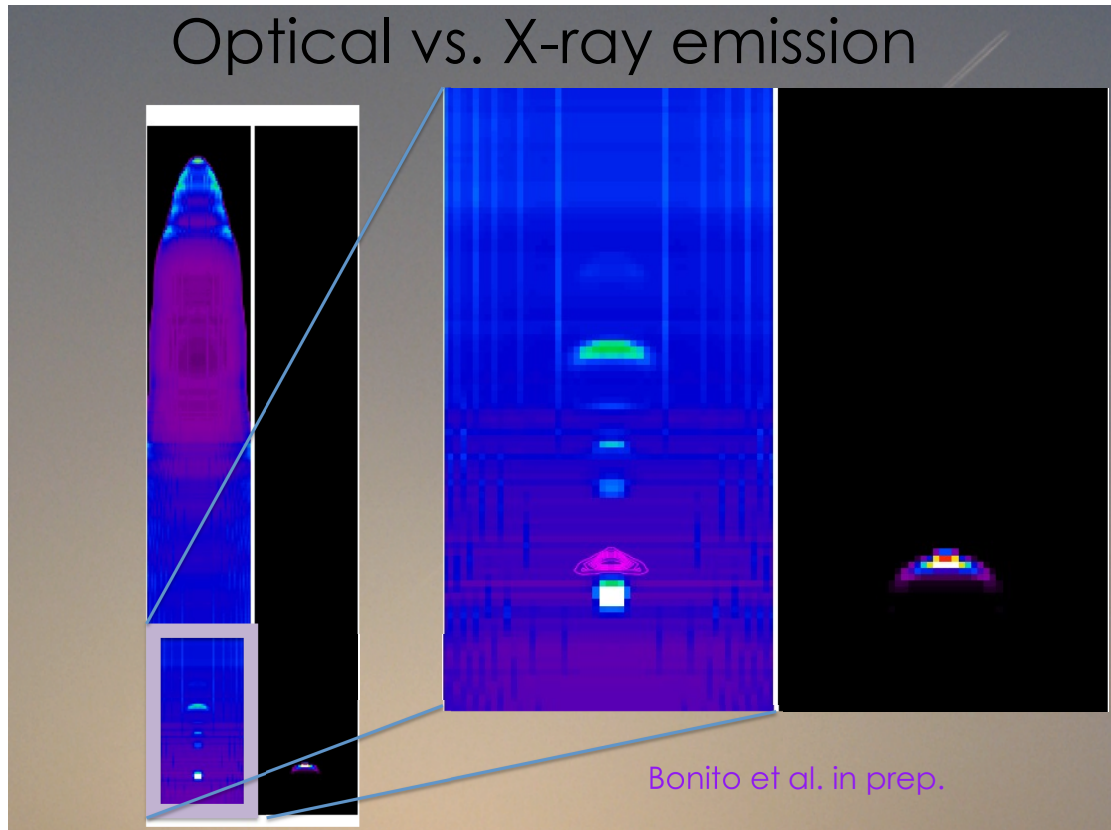


Figure 1: Emission maps synthesized from the model of a pulsed jet. Both the optical (left panels) and the X-ray emission (right panels) can be derived from the model to be compared with the observations. The enlargement on the right shows the stratification of the high energy source detected at the base of the jet and the chain of optical knots along the jet axis.

## THE CHEMICAL INVENTORY OF HH1

T. Giannini; *INAF - Osservatorio Astronomico di Roma, Monte Porzio Catone, Italy.*

Protostellar shocks exert a profound impact in the interstellar medium, provoking irreversible changes in its physical and chemical composition and ionization degree. We have exploited the X-shooter sensitivity to observe the prototype protostellar shock, i.e. the Herbig-Haro object HH1 ( $\alpha_{J2000.0}=05^h 36^m 20^s 27$ ,  $\delta_{J2000.0}=-06^\circ 45' 04'' 84$ , distance of 414 pc). Our aims are to: 1) provide the most complete atlas of the chemical species involved in protostellar shocks; 2) obtain a detailed picture of the gas physical conditions that will be used as a benchmark for shock models; 3) understand the ability of shocks to destroy dust and enhance the gaseous phase abundance of the refractory species.

The target was observed during several nights between November 2013 and January 2014, for a total integration time on-source of  $\sim 3.5$ h in the range 3 000-24 700 Å (for details see [1]). The spectrum is extraordinary rich in emission lines, with more than 500 detections of fine structure ionic lines from species with  $Z \leq 28$ , HI recombination lines of the Balmer, Paschen, and Brackett series, several He recombination lines, and  $H_2$  ro-vibrational lines with  $v_{up} \leq 9$ . The analysis of the HH1 spectrum consists of the following steps: 1) derivation of the local extinction ( $A_V$ ); 2) derivation of the gas physical conditions; 3) estimate of the chemical abundances of the atomic species.

The local extinction was derived from ratios of lines coming from the same levels [1,2]. In particular, from very bright HI ratios of the Balmer and Paschen series, we got  $0.0 \leq A_V \leq 0.8$  mag. Temperature and density of the emitting gas were fitted for each species by applying a Non Local Thermal Equilibrium (NLTE) model, which considers collisional excitation and de-excitation and spontaneous decay as processes responsible for the line emission. The main result of this part of the analysis is summarized in Figure 1 ([3]). Here the electron temperature (black data) is plotted as a function of  $IP_{ave}=(IP_{i-1}+IP_i)/2$ , i.e. the average between the ionization potentials of the ionic states  $i-1$  and  $i$ . This gives an idea of the energy range corresponding to the ionization stage  $i$  of the considered species. Notably, the electron temperature is not constant, but rather spans in the range 5 000-90 000 K. Moreover, we find a strong correlation between the ionization energy of the ion under consideration and the derived  $T_e$ . Conversely, two different regimes of density can be individuated: a more tenuous component with  $n_e$  between  $1.0 \cdot 10^3 \text{ cm}^{-3}$  and  $5.0 \cdot 10^3 \text{ cm}^{-3}$ , probed by low-ionized atoms, and a denser gas component, with  $n_e \geq 1.0 \cdot 10^5 \text{ cm}^{-3}$ , probed by high-ionized atoms, with a tendency of this latter to be also at higher temperature. To derive the fractional ionization  $x_e = n_e/n_H$  and the fractional ionic abundance  $X^i/X^{i+1}$  of each species, we developed a ionization code that takes into account the following processes: direct ionization, radiative and dielectronic recombination and direct and inverse charge-exchange with hydrogen. In Figure 1 red data represent  $x_e$  vs.

$IP_i$ . Although the data points are few, a clear stratification in  $x_e$  is recognizable, being the gas substantially neutral for  $IP_i \leq 10$  eV (and  $T_e \leq 20\,000$  K) up to be completely ionized for  $IP_i \geq 40$  eV (and  $T_e \geq 40\,000$  K).

To derive the chemical abundances of the detected species, we considered ratios of bright atomic lines with the  $H\beta$  line for species having  $T_e \leq 30\,000$  K and the HeII 4-3 line in the opposite case. The observed ratios were compared with the intensities predicted at the derived  $T_e$ ,  $n_e$ , and  $x_e$ . As a general result, we get abundances significantly lower both than the solar values ([4]) and the estimates in the Orion nebula ([5]). This trend is even emphasized for refractory species (C, Ca, Ti, Fe, Ni) which abundance is on average around 50% less than the solar value. This result can be interpreted in terms of the shock efficiency, which in HH1 as in other protostellar shocks (e.g.[6],[7]), is not enough to completely destroy dust.

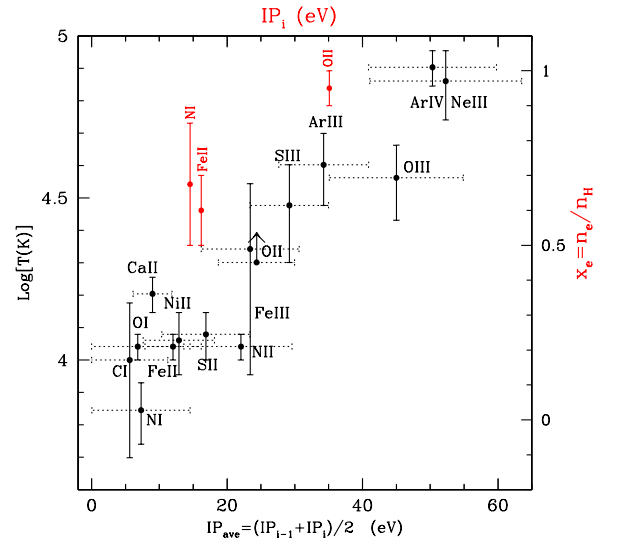


Figure 1: Black/Red:  $T_e/x_e$  as fitted with the excitation/ionization model as a function of the ionization potential.

### References.

- [1] Giannini, T., Antonucci, S., Nisini, B., et al. 2015, *ApJ*, 798, 33
- [2] Gredel, R. 1994, *A&A* 292, 580
- [3] Giannini, T., et al., in preparation
- [4] Asplund, M., Grevesse, N., & Sauval, A. J. 2005, *Cosmic Abundances as Records of Stellar Evolution and Nucleosynthesis*, 336, 25

- [5] Esteban, C., Peimbert, M., García-Rojas, J., et al. 2004, MNRAS, 355, 229
- [6] Podio, L., Medves, S., Bacciotti, F., Eislöffel, J., & Ray, T. 2009, A&A, 506, 779
- [7] Giannini, T., Nisini, B., Antonucci, S., et al. 2013, ApJ, 778, 71

## CONNECTION BETWEEN JETS, WINDS, AND ACCRETION IN T TAURI STARS

B. Nisini; *INAF - Osservatorio Astronomico di Roma, Monte Porzio Catone, Italy.*

The standard paradigm for the formation of low-mass stars is that powerful jets and/or winds are formed during the early stages of stellar evolution as a mechanism to extract the excess angular momentum from the system, allowing accretion of matter from the disk onto the star. Several mass ejection phenomena from active T Tauri stars (Classical T Tauri, CTT stars) are indeed detected using different tracers/techniques. The most clear evidence of mass loss are the collimated and extended jets observed in optical narrow band images. Such high velocity jets can be also easily spotted in the spectra of their driving source through the detection of forbidden emission lines (red- or blue-shifted, with velocities  $> 40\text{--}50\text{ km s}^{-1}$ ) of abundant species, such as [OI], [SII], [NII], [FeII], which span a wide range of wavelengths from UV to IR (e.g. [5]). This emission is usually referred to as the High Velocity Component (HVC). In addition to this HVC, spectra of T Tauri stars exhibit forbidden line emission at low velocity ( $< 40\text{ km s}^{-1}$ ) which is not spatially resolved (the so-called low velocity component, or LVC). The origin of this component is less clear; suggestions are that it could originate from a slow disk-wind or from photo-evaporating wind driven by high-energy photons from the central star [6,9]. Finally, the presence of hot stellar winds is often testified by the prominent P-Cygni absorption profile shown by many CTT in the He I  $1.08\mu\text{m}$  line [4]. The above emissions have been separately investigated and discussed in several studies, however rarely the different mechanisms have been related together and connected with the accretion properties of the central star in a unified picture.

We present here a statistical investigation on the occurrence of different jets/winds tracers and their mutual relationship based on spectra acquired at VLT with the X-shooter instrument. These data, covering in a single exposure the spectral range from UV to near-IR, allow us to simultaneously observe the main tracers of both high velocity jets, winds and accretion signatures. The so far considered sample is composed by CTTs in three star forming regions, namely Lupus, Chameleon and  $\sigma$  Ori. The X-shooter spectra of Lupus and  $\sigma$  Ori (44 sources) are presented in [1] and [8], where their accretion and stellar properties have been derived. The properties of their LVC emission has been instead discussed in [7]. The Chameleon sample comprises 16 sources selected from the objects investigated in [2]. All together, the global sample of 60 sources spans a mass range between  $0.03$  and  $2\text{ M}_{\odot}$ , and mass accretion rates from  $2.5\text{ }10^{-12}$  to  $1\text{ }10^{-7}\text{ M}_{\odot}/\text{yr}$ .

The most common forbidden line in the spectra is the [OI]6300Å detected in 87% of the sources. This emission is more often related to a LVC (peak velocity  $< 40\text{ km s}^{-1}$ ), while only 32% of the sources present an HVC (peak velocity  $> 40\text{ km s}^{-1}$ ). Thus only  $\sim 1/3$  of the considered sources do show a high velocity jet, although this number could be higher due to orientation effects. We have investigated if the sub-sample of sources with HVC emission present peculiarities

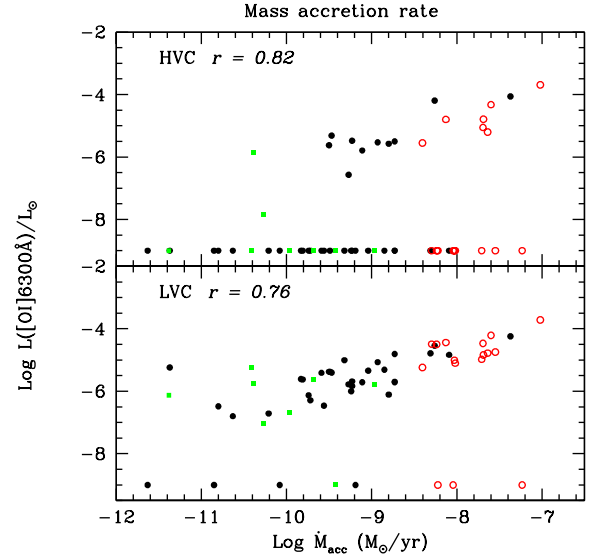


Figure 1: Correlation between [OI]6300Å luminosity and mass accretion rate for sources of our sample in the Lupus (black),  $\sigma$  Ori (green) and Chameleon (red) star forming regions. The line luminosity has been separately plotted for the LVC (lower panel) and HVC (upper panel). The corresponding correlation coefficient is given in each panel. For sources where the [OI] line is not detected in one of the two components, its luminosity has been artificially settled to  $10^{-9}\text{ L}_{\odot}$ .

with respect to the rest of the sources and if their LVC is influenced in some way by the jet presence. To do that, we have performed a series of correlations between the extinction corrected [OI] line luminosity, separately computed for the HVC and LVC through gaussian line fitting, and accretion and stellar parameters. As an example, in Fig. 1 we show the correlation between the line luminosity and the source mass accretion rate (derived in [1,9,2]). The line luminosity correlates with  $\dot{M}$  for both the LVC and HVC, however there is a significant number of high accretors that do not have any detected HVC. In practice, only about half of sources with  $\dot{M} > 10^{-9}\text{ M}_{\odot}/\text{yr}$  show evidence of a high velocity jet. Similar correlations have been found between [OI] luminosity and other stellar parameters, such as mass and luminosity, without finding any segregation of sources without HVC in specific ranges of parameter space. Similarly, there is no difference in line luminosity or kinematics (e.g. velocity peak or line width) of the LVC in sources with and without the HVC.

In the assumption that all protostars develop jets during the earliest phases of their formation, the above findings suggest that jets and disk accretion do not evolve with the same

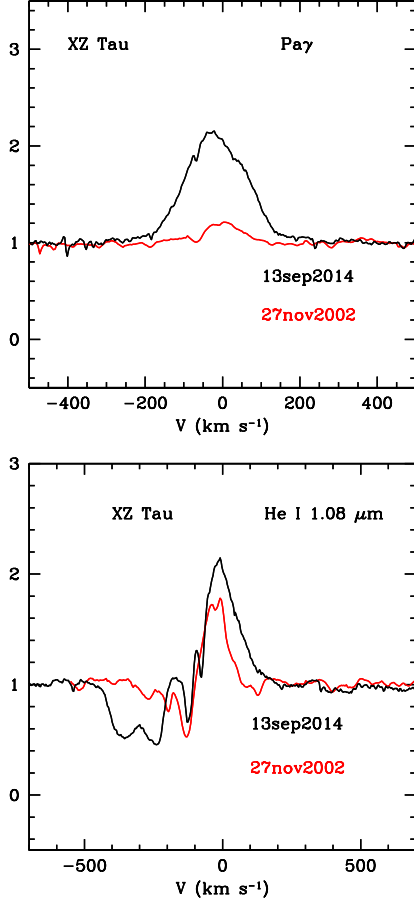


Figure 2: GIANO continuum-normalized observations of the HeI  $1.08\mu\text{m}$  and  $\text{Pa}\gamma$  lines of XZ Tau taken in sept. 2014 (black line) compared with spectra of the same lines taken during 2002 at Keck II [4]. The recent increase in the  $\text{Pa}\gamma$  EW, likely caused by an accretion event, is followed by an increase in the HeI emission component as well as by a widening of the blue-shifted absorption component, suggesting that the stellar wind is directly driven by accretion.

timescales, but high velocity jets are dissipated while the star is still accreting. In addition, high velocity jets and slow winds seem to be unrelated, since the properties of slow winds are not influenced by the jet presence.

We have also searched for the presence of P-Cygni ab-

sorption in the HeI  $1.08\mu\text{m}$  line of our sample, in order to correlate the hot stellar winds traced by this line with the slow and high velocity winds/jets probed by the [OI] LVC and HVC. Only 19/60 sources have a detectable P-Cygni absorption, a result that can be biased by the limited spectral resolution ( $R \sim 8000$ ) that prevents the detection of the weak features. For these sources, we find a weak correlation between [OI] luminosity and the blue-shifted absorption EW, for both the HVC and LVC. Similarly, such EW only weakly correlates also with the accretion luminosity of the sources (correlation coefficient 0.5). Such correlations would need to be better confirmed on a larger sample than analysed here.

A direct evidence that the depth of the HeI  $1.08\mu\text{m}$  blue-shifted absorption is correlated with accretion comes from high resolution near-IR spectra acquired with the GIANO instrument ( $R \sim 50\,000$ ) at TNG on the EXor variable source XZ Tau. Fig. 2 shows the recently obtained GIANO spectra in the HeI and  $\text{Pa}\gamma$  lines, as compared with the spectra of the same lines acquired in a different epoch by [4]. The recent spectra show a large increase in the  $\text{Pa}\gamma$  equivalent width accompanied by an increase of the HeI emission component. At the same time the depth and maximum velocity of the blue-shifted absorption component are much larger than before. These observations suggest that the source had an accretion burst (testified by the  $\text{Pa}\gamma$  increase) accompanied by the ejection of a stronger stellar wind (deeper absorption in a larger velocity range).

#### References.

- [1] Alcalá, J., Natta, A., Manara, C., et al. 2014, A&A, 561, 2
- [2] Antonucci, S., García López, R., Nisini, B., et al. 2011, A&A, 534, A32
- [3] Edwards, S., Fischer, W., Kwan, J., Hillenbrand, L., & Dupree, A. K. 2003, ApJ, 599, L41
- [4] Edwards, S., Fischer, W., Hillenbrand, L., Kwan, J. 2006, ApJ, 646, 319
- [5] Hamann, F. 1994, ApJSS, 93, 485
- [6] Hartigan, P., Edwards, S., & Ghandour, L. 1995, ApJ, 452, 736
- [7] Natta, A., Testi, L., Alcalá, J. M., et al. 2014, A&A, 569, A5
- [8] Rigliaco, E., Natta A., Testi L., et al. 2012, A&A, 548, 56
- [9] Rigliaco, E., Pascucci, I., Gorti, U., Edwards, S., & Hollenbach, D. 2013, ApJ, 772, 60

## **Part 4:**

### ***Physical and Chemical Properties of Disks***

# DISKS AND JETS WITH ALMA: SCULPTING THE BIRTHPLACE OF EXOPLANETS

Linda Podio; *INAF - Osservatorio Astrofisico di Arcetri, Firenze, Italy.*

The first step to comprehend the formation of our solar system as well as of extra-solar planetary systems is to study the evolution of the planet formation site: the circumstellar disk. To understand how disks lose their mass and form protoplanets is a front line in astrophysics. These processes are believed to be regulated by the simultaneous effects of the mass accretion onto the star and the ejection of matter from the stellar-disk system. However, the interface between jets and disks has been poorly investigated to date because of both the very small angular scales involved and the occurrence of numerous other kinematic components in the circumstellar region (cavities of swept-up material, infalling envelope, static ambient cloud). The Atacama Large Millimeter Array (ALMA) with its unprecedented combination of angular resolution and sensitivity offers us for the first time the opportunity to simultaneously probe the disk *and* the jet in embedded protostars.

The HH 212 protostellar system in Orion (at 450 pc) is an ideal laboratory to investigate the interplay of infall, outflow and rotation in the earliest evolutionary phases of the star-forming process. HH 212 is low-mass Class 0 source driving a symmetric and bipolar jet extensively observed in typical molecular tracers such as H<sub>2</sub>, SiO, and CO (e.g., [14]). Observations of the HH 212 protostar in SO 9<sub>8</sub> – 8<sub>7</sub> and 10<sub>11</sub> – 10<sub>10</sub> lines have been performed using ALMA-band 7 extended configuration (Cycle 0). The obtained data-cubes have a spectral resolution of 488 kHz (0.42 – 0.43 km s<sup>-1</sup>), a typical beam FWHM of 0.65'' × 0.47'' at PA ~ 49°, and an rms noise of ~ 3 – 4 mJy/beam in the 0.43 km s<sup>-1</sup> channel.

The channel maps presented in Figure 1 show that SO 9<sub>8</sub> – 8<sub>7</sub> traces different components in the inner ~ 1300 AU of the HH 212 protostellar system: (i) the X-shaped cavity walls at systemic velocity; (ii) the poorly collimated outflow (width ~ 135 AU) swept out by the jet at low velocities; (iii) the collimated ( $R_{jet} \sim 90$  AU) and fast ( $V_{jet} \sim 100 - 200$  km s<sup>-1</sup>) molecular jet at intermediate and high velocities. Conversely, the emission in the high-excitation SO 10<sub>11</sub> – 10<sub>10</sub> line presented in Figure 2 shows a compact structure with the blue- and the red-shifted peaks displaced roughly on the equatorial plane, which is consistent with an origin in the 90 AU disk rotating around a ~ 0.2 – 0.3 M<sub>⊙</sub> star previously detected by [7] and [2].

The ALMA observations show that SO emission at high-velocity can be used as an effective probe of the molecular jet, similarly to a standard tracer such as SiO (see also [8,13,3]). The high velocity molecular jet is dense (~ 10<sup>5</sup> – 10<sup>6</sup> cm<sup>-3</sup>) and transports a mass loss rate ≥ 0.2 – 2 × 10<sup>-6</sup> M<sub>⊙</sub> yr<sup>-1</sup>, indicating a high ejection efficiency (≥ 0.03 – 0.3, for an

infall rate of ~ 6 × 10<sup>-6</sup> M<sub>⊙</sub> yr<sup>-1</sup>, [9]). The SO abundance in the jet (~ 10<sup>-7</sup> – 10<sup>-6</sup>) is similar to what estimated in other Class 0 outflows and jets (e.g., [1,13,8]) and indicates that 1% to 40% of the elemental S has been converted into SO in the shocks along the jet (e.g., [6]) and/or at the base of the wind due to ambipolar diffusion [10].

The disk mass derived from C<sup>17</sup>O 3–2 is ≥ 0.002 – 0.013 M<sub>⊙</sub>, which is consistent with what inferred from HCO<sup>+</sup> by [7]. The SO abundance (~ 10<sup>-8</sup> – 10<sup>-7</sup>) is 3 – 4 orders of magnitude larger than what estimated in evolved protoplanetary disks (e.g., [5]). Such an SO enhancement may be produced in the accretion shock occurring at the interface between the envelope and the disk [7,12], or in spiral shocks if the disk is partly gravitationally unstable (e.g., [4]). Higher angular resolution and sensitivity observations are required to address the exact origin of the high-excitation SO emission.

## References.

- [1] Bachiller, R. & Perez Gutierrez, M. 1997, ApJ, 487, L93
- [2] Codella, C., Cabrit, S., Gueth, F., et al. 2014, A&A, 568, L5
- [3] Codella, C., Maury, A. J., Gueth, F., et al. 2014, A&A, 563, L3
- [4] Douglas, T. A., Caselli, P., Ilee, J. D., et al. 2013, MNRAS, 433, 2064
- [5] Dutrey, A., Wakelam, V., Boehler, Y., et al. 2011, A&A, 535, A104
- [6] Flower, D. R., & Pineau des Forets, G. 1994, MNRAS, 268, 724
- [7] Lee, C.-F., Hirano, N., Zhang, Q., et al. 2014, ApJ, 786, 114
- [8] Lee, C.-F., Hasegawa, T. I., Hirano, N., et al. 2010, ApJ, 713, 731
- [9] Lee, C.-F., Ho, P. T. P., Beuther, H., et al. 2006, ApJ, 639, 292
- [10] Panoglou, D., Cabrit, S., Pineau Des Forets, G., et al. 2012, A&A, 538, A2
- [11] Podio, L., Codella, C., Gueth, F., et al. 2015, A&A, in press (arXiv:1505.05919)
- [12] Sakai, N., Sakai, T., Hirota, T., et al. 2014, Nat, 507, 78
- [13] Tafalla, M., Santiago-García, J., Hacar, A., & Bachiller, R. 2010, A&A, 522, A91
- [14] Zinnecker, H., McCaughrean, M. J., & Rayner, J. T. 1998, Nature, 394, 862

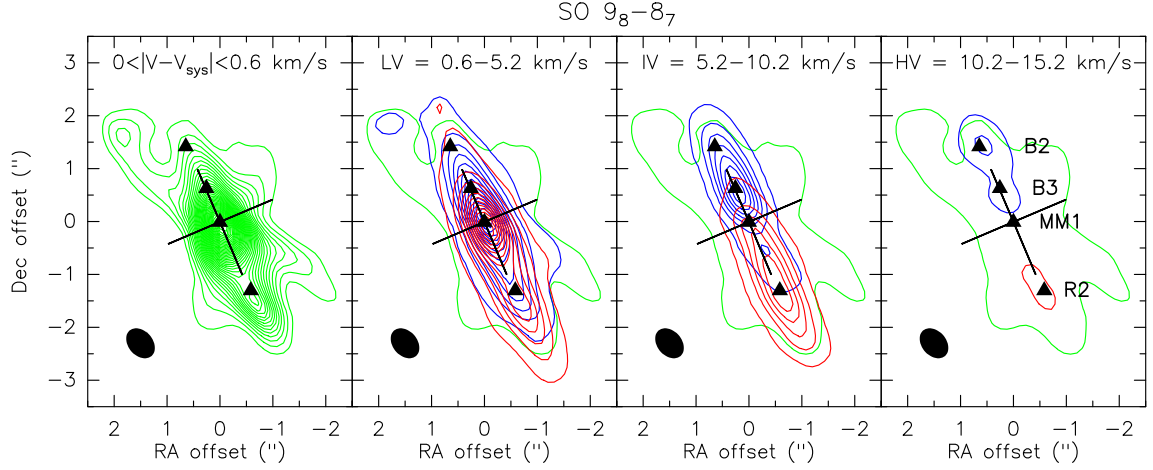


Figure 1: Channel maps of SO  $9_8 - 8_7$  at systemic, low (LV), intermediate (IV), and high (HV) velocities (*panels from left to right*). The green, blue, and red contours trace the emission at systemic velocity and over the labeled blue- and red-shifted velocity intervals ( $|V - V_{sys}|$ ). The lowest contour of the emission at systemic velocity is shown in all panels. The first contour is at  $5\sigma$  for SO and  $3\sigma$  for SO<sub>2</sub> with steps of  $5\sigma$  ( $V_{sys}$ ) and  $20\sigma$  (LV, IV, HV) for SO and  $3\sigma$  for SO<sub>2</sub> ( $1\sigma \sim 3-4$  mJy/beam/ $0.43$  km s<sup>-1</sup>). The tilted black cross is centred at the source position and indicates the jet and the disk PA ( $PA_{jet} = 22^\circ$ ,  $PA_{disk} = 112^\circ$ ). The ellipse in the bottom-left corner shows the beam HPBW of the line emission maps ( $0.65'' \times 0.47''$ ,  $PA = 49^\circ$ ). The triangles indicate the emission peaks along the blue and red lobes. Adapted from [11].

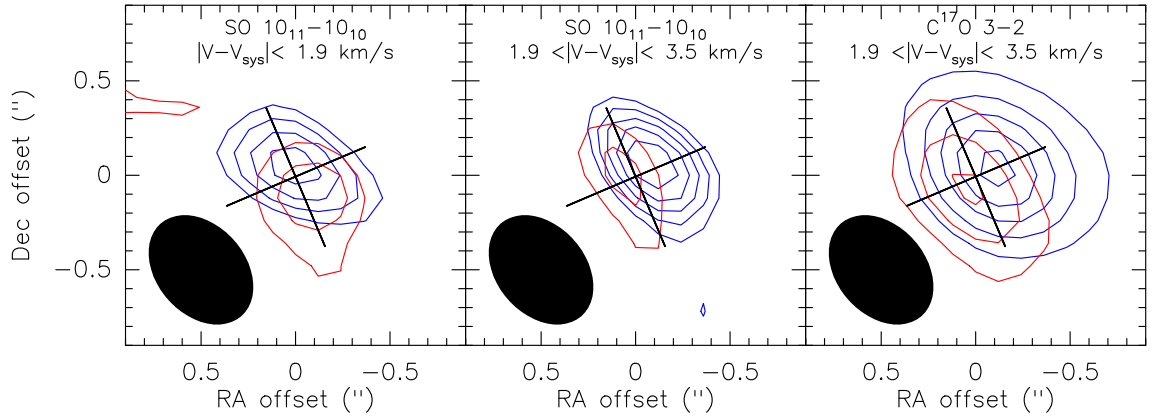


Figure 2: Blue- and red- shifted emission of SO  $10_{11} - 10_{10}$  at low velocities ( $|V - V_{sys}| < 1.9$  km s<sup>-1</sup>, *left panel*) and in the higher velocity range where the emission is consistent with a rotating disk ( $HV_{disk} : 1.9 < |V - V_{sys}| < 3.5$  km s<sup>-1</sup>, *middle panel*) is compared with C<sup>17</sup>O  $3 - 2$  emission in the  $HV_{disk}$  range (*right panel*, [2]). The tilted black cross indicates the jet ( $PA = 22^\circ$ ) and the disk ( $PA = 112^\circ$ ) direction. The ellipse in the bottom-left corner shows the beam HPBW of the line emission maps ( $0.65'' \times 0.47''$ ,  $PA = 49^\circ$ ). First contour at  $5\sigma$  with steps of  $5\sigma$  for C<sup>17</sup>O  $3 - 2$  and at  $3\sigma$  with steps of  $1\sigma$  for SO  $10_{11} - 10_{10}$ . Adapted from [11].

# A NEW FITTING TOOL TO CONSTRAIN DUST GRAIN SIZE DISTRIBUTION AND DISK PROPERTIES WITH ALMA AND JVLA OBSERVATIONS

M. Tazzari<sup>1,2</sup>, L. Testi<sup>1,2,3</sup>, B. Ercolano<sup>2,4</sup>, A. Natta<sup>3,5</sup>; <sup>1</sup>*European Southern Observatory, Garching bei München, Germany*, <sup>2</sup>*Excellence Cluster Universe, Garching bei München, Germany*, <sup>3</sup>*INAF - Osservatorio Astrofisico di Arcetri, Firenze, Italy*, <sup>4</sup>*Universitäts-Sternwarte München, Germany*, <sup>5</sup>*Dublin Institute for Advanced Studies, Dublin, Ireland*.

## 1. Introduction

Current planet formation models propose two possible mechanisms to explain the variety and the large number of planetary systems observed so far (for a review of exoplanets properties, see [1]): the so-called *core accretion* scenario, in which planets are formed through a process of slow accumulation of solids into planetesimals and rocky cores followed by gas accretion; or the *gravitational instability* scenario, in which planetary mass objects are formed by the exponential growth of instabilities in the disk. Furthermore, the Kepler mission and recent meteoritic studies suggest that the *core accretion* scenario is playing an important role for many systems, supporting the view that small rocky bodies are assembled by collecting grains and pebbles that grow throughout the life of the protoplanetary disk [2].

## 2. Assessing the dust grain size

The first step of planet formation in the *core accretion* scenario is the growth of dust to form large aggregates and eventually planetesimals (see [3] for a recent review). This first phase of growth from ISM-sized particles to mm-sized pebbles is directly observable in the disk midplane by measuring the dust opacity  $\kappa_\nu$  as a function of wavelength in the millimetre domain (e.g. [4]).

At (sub-)mm wavelength the disk emission is mostly optically thin and can be written as

$$F_\nu \propto B_\nu(T)(1 - e^{-\tau}) \approx \nu^2 \kappa_\nu \Sigma T, \quad (1)$$

where  $\kappa_\nu$ ,  $\Sigma$  and  $T$  are respectively the dust opacity, the dust surface density and the local disk temperature. Assuming a dust grain size distribution  $n(a) \propto a^{-q}$  for  $a_{\min} < a < a_{\max}$ , it is possible to show that the dust spectral index  $\beta$  (defined as  $\kappa_\nu \propto \nu^\beta$ ), depends on  $a_{\max}$  only (provided that  $a_{\min} < 1\mu\text{m}$ , see [5]). According to Eq. (1), the slope  $\alpha_{\text{mm}}$  of the (sub-)mm SED ( $F_\nu \propto \nu^{\alpha_{\text{mm}}}$ ) is related to the dust opacity spectral index  $\beta$  simply as  $\alpha_{\text{mm}} \approx \beta + 2$ . As a conclusion, from (sub-)mm multi-wavelength observations is possible to directly estimate the level of grain growth ( $a_{\max}$ ) in the disk midplane through the measure of  $\alpha_{\text{mm}}$ . Typical values of  $\alpha_{1-3\text{mm}} \sim 3.7$  are found for the relatively small ISM dust grains ( $a_{\max} \approx 0.25\mu\text{m}$ , see [5]), while [6] showed that dust grains with sizes  $a_{\max} \geq 1\text{mm}$  lead to  $\beta \leq 1$  ( $\alpha_{1-3\text{mm}} \leq 3$ ), regardless of the dust composition, porosity and size distribution.

## 3. A multi-wavelength fitting tool

In order to constrain the dust grain size distribution in a protoplanetary disk, we have developed a fitting tool that aims at fitting multi-wavelength (sub-)mm interferometric observations with a self-consistent modeling of the dust opacity and

the disk structure. The tool fits directly the observed visibilities in order to avoid possible nonlinear artifacts introduced by the CLEAN algorithm. Fitting multi-wavelength observations allows to break the degeneracy in the terms on the right hand side of Eq. (1), namely  $\kappa_\nu(R)$ ,  $\Sigma(R)$  and  $T(R)$ .

The disk emission  $F_\nu$  is modeled with a classical two layers disk model (see [7]) assuming a parametrization for the disk surface density  $\Sigma(R) = \Sigma_0 (R/R_0)^{-\gamma} \exp[-(R/R_c)^{2-\gamma}]$ , where  $\Sigma_0$  is a constant,  $R_0 = 40\text{ AU}$  and  $R_c$  is the spatial scale of the exponential cutoff. We also parametrize the maximum dust grain size in the midplane as  $a_{\max}(R) = a_{0\max}(R/R_0)^{b_{\max}}$  (whereas  $a_{\min}$  is kept fixed throughout the disk). Therefore the disk model has five free parameters:  $\gamma$ ,  $\Sigma_0$ ,  $R_c$ ,  $a_{0\max}$ ,  $b_{\max}$ .

To perform the fit we adopt a bayesian approach, using an affine invariant Markov Chain Monte Carlo (MCMC) algorithm, highly efficient for multi-dimensional problems and designed for highly parallel computations (we use the implementation of the *emcee* Python package, see [8]). The resulting MCMC provides estimates of the posterior distribution function in the five-dimensional space of parameters, out of which we can compute the marginalized distributions (to infer the values for each parameter) and the bivariate distributions (to investigate correlations between the parameters).

We have successfully applied this fitting tool on ALMA, CARMA, SMA and EVLA observations of disks from the Disks@EVLA sample (PI: C.Chandler, NRAO), mainly from the Taurus star-forming region. For each disk, we have fitted simultaneously four to six observations at wavelengths ranging from 0.8 mm to 1 cm. In almost all the cases we have reported  $\beta(R)$  profiles that increase with radius, from  $\beta \ll 1$  at  $R \leq 40\text{ AU}$  to  $\beta > 1.5$  in the outer disk, and accordingly  $a_{\max}(R)$  decreasing with radius, with  $a_{\max} \approx 1\text{ cm}$  at  $R \leq 40\text{ AU}$  and  $b_{\max} \approx -1$ . These results confirm theoretical expectations from dust evolutionary models that predict the smaller dust particles to be diffused throughout the disk and the larger pebbles to be driven to the inner disk by the gas drag. This analysis is still statistically limited by the number of disks that have been analysed (less than ten), however a future analysis on larger samples of disks will allow to investigate possible correlations between the dust processing level and the stellar parameters.

## References.

- [1] Lissauer et al. 2014, Nature 513, 336
- [2] Connelly et al. 2012, Science 338, 651
- [3] Testi et al. 2014, PPVI, 339
- [4] Beckwith & Sargent 1991, ApJ 381, 250

[5] Draine 2006, ApJ 636, 1114

[6] Natta & Testi 2004, ASP Conf. S. 323, 279

[7] Dominik et al. 2001, ApJ 560, 957

[8] Foreman-Mackey et al. 2013, PASP 125, 306